AMT-2019-100
Responses to reviews

Mason, S., Hogan, R, Westbrook, C., Kneifel, K., Moisseev, D. and von Terzi, L.

August 5, 2019

We thank the reviewers for their constructive feedback on the manuscript. A recurring suggestion was that we apply the retrieval to more data than the 25-minute case study from 21 February 2014 originally used. We agree that this is desirable, reiterating that while the colocated remotely-sensed and in situ measurements of snow from BAECC 2014 are extremely valuable and of a high quality, the number of cases are limited. A related comment was that we should more clearly acknowledge the limited measurement period to which our retrieval was applied. In addressing both of these suggestions, we have both included an additional case study and de-emphasised the retrieval of the PSD shape parameter in discussing the results.

During the snow experiment intensive observation period of BAECC there were three cases in which all three radars were zenith-pointing during a snow event, and where the snowfall at the surface was not affected by melting (the cases shown in Kneifel et al. 2015). The snowfall at the surface during one of these cases (7 February 2014) was insufficient for the in situ snow retrieval of von Lerber et al. (2015). We have therefore expanded our study to include 60 minutes of snowfall from the 16 February 2014 case. This case also includes riming, but is notable for the presence of secondary ice production due to rime splintering (the Hallett-Mossop process). These secondary needles rapidly aggregate, such that the radar measurements in this case are dominated by large aggregate snowflakes with a very open structure, while the in situ measurements include a mixture of graupel, large aggregates, and needles.

In applying our retrieval to this case, it was evident from PIP measurements that the PSD shape was nearly constant, but that significant changes in the triple-frequency radar signature could be attributed to the presence of large aggregates of needles, consistent with the findings of Leinonen and Moisseev (2015). We have therefore expanded the scope of the study to include the effects of variations in the internal structure of aggregates, which are represented within the SSRGA. We hope the reviewers agree that expanding the study to address both the PSD shape parameter and the internal structure of aggregates strengthens this effort to better understand and interpret the parameters affecting triple-frequency radar measurements.

To summarise, we have made the following changes:

- The title is now, "The importance of particle size distribution and internal structure for triple-frequency radar retrievals of the morphology of snow"
- We added a coauthor, Leonie von Terzi at the University of Cologne.
- We expanded our discussion of the coefficients of the SSRGA, especially those relating to the internal structure of aggregate particles, in Sections 2.1 and 3. L. von Terzi's contribution to the study was to perform simulations of aggregation of various monomers and their SSRGA coefficients; we use this to identify aggregates of needles as having triple-frequency radar signatures with especially low values of DWR_{35-95} compared to aggregates of other monomers.
- Section 5 now uses the 16 February case study to explore triple-frequency radar measurements and retrievals from a case featuring rime splintering. This is a very distinct situation from the first case study, and combined the two cases cover the wide range of triple-frequency radar measurements from during BAECC 2014.
- The discussion and conclusions (Section 6) have been substantially re-written to be more concise, while addressing the expanded scope of the paper.

Reviewer #1

Specific comments

This may be personal preference, but throughout the paper "PSD shape" is used to refer to the parameter μ–while I understand in the normalized distribution space μ does modify the actual

shape (width) of the distribution, when talking about μ I think it may be clearer to refer to this as the "PSD shape factor" or "PSD shape parameter", as done on P4 L9.

We agree that this is most consistent and clear, and now refer everywhere to "PSD shape parameter".

P2 L30-L32: Are triple-frequency measurements always at precisely 95 GHz, 35GHz, and a third frequency below 15 GHz? Or is that just what is used in this study? I would consider modifying this sentence to say something like "Typically,..." or "In this study,...".

Good point. In the literature on triple-frequency signatures of snow this configuration of radars is typical. However, it's true that the lowest frequency radar have been any of C, X or Ku-bands radars. The sentence now reads:

> The triple-frequency radar 'signature' consists of radar measurements at three frequencies spanning the millimeter wavelength range, the two dual-wavelength ratios (DWRs) ~~derived from radar measurements~~ of which reveal information about non-Rayleigh scattering from larger snowflakes. Typically radars at 95, ~~35-GHz~~ 35 and a third frequency ~~below 15-GHz, and provides~~ between 3 and 15 GHz are used [e.g. *Kneifel et* al., 2015; *Leinonen and Szyrmer*, 2015; *Barrett et* al., 2019]

P3 L13-L14: This sentence needs some clarification, as numerous studies have already been described that employ triple-frequency radar retrievals. Can the exact novel aspect of this study's triple-frequency radar retrieval be stated more clearly here?

Indeed, the novelty is that both the triple-frequency radar reflectivity factors and mean Doppler velocity measurements are assimilated in order to estimate different aspects of the particle morphology. This sentence now reads,

> To our knowledge ~~, a~~ a retrieval assimilating both triple-frequency ~~Doppler retrieval of ice~~ radar reflectivity factors and mean Doppler velocity to estimate the properties of snow has not yet been ~~described – this may~~ described. This approach should have the advantages of ~~estimating particle density constrained by~~ constraining particle density with Doppler velocity [as in *Mason et al.*, 2018]~~and~~ , while using triple-frequency radar signatures to constrain some ~~parameters of particle morphology~~additional parameter affecting the microphysical properties or size distribution of precipitating ice particles.

P4 L16-17: This sentence is a bit confusing. Given the description of the assumptions on how each particle is treated (e.g., as a homogenous spheroid) when calculating the radar backscatter cross-sections, it might be clearer to state something along the lines of, "Approximations of the microphysical structure are used to calculate the radar backscatter cross-section", or, "The microphysical structure is represented through an approximation when calculating the radar backscatter cross-section".

We agree. The sentence now reads,

> The morphology of ~~the~~ ice particles is represented by ~~three~~ parameters controlling their microphysical structure, density, and shape. ~~The microphysical structure is represented in an approximation to~~ Approximations to the microphysical structure of ice particles are used to calculate the radar backscatter cross-section ~~$\sigma(D)$~~ (σ) of each particle.

Figure 2: There should be boxes around the legends, particularly in panel (b) to differentiate it from actual data points. It should also be clarified that the y-axis units in(a) are in linear units (or convert them to log units) since it was previously stated DWR would be expressed in dB. Finally, the y-axis labels have no context – what is f? For(a), either explain in the caption or just convert it to dB, since DWR has already been explained in the text, and for (b) perhaps just state "Volume-Weighted Concentration".

We have modified the titles and y-axis labels of both subplots to make the quantities clearer, and have added an equation to define the dual-backscatter ratio (DBR) consistent with Kneifel et al. 2016, and which is now shown in dB. Boxes have been also added to the legends in plot (b).

P9 L29: "... The many narrow features of the backscatter cross-section ratio spectra are smoothed out" should have "when integrated across the PSD" added to it.

This is indeed clearer. We've made the change.

P14 L1-L4: I was initially confused with how this differed from the analysis presented in Figure 1, but gathered later that the PSD shape factor and density factor used were informed by the observed precipitation. I suggest making that fact more explicit and putting it earlier in the section.

Thank you, this was helpful feedback. To better highlight the important information in each figure, we no longer overlay the triple-frequency signatures with triple-frequency radar measurements in the first figure. This makes it easier in this figure to interpret how the triple-frequency radar signatures for different particle types change with the physical parameters, and leaves the comparison with measurements to the case studies (Figs. 7 & 12).

P14 L10: It looks to me like the frontal snow regime has DWR10-35 exceeding 10dB?

Thank you, we've made this change.

P16 L24: The sentence "the state vector is linearly interpolating between the retrieved state vectors at the retrieved value of PSD shape..." is unclear to me. Once the optimal μ value is found, which state vectors is the "retrieved" state vector interpolated between? Also, should "found by" be before "linearly interpolating"?

This sentence was not only unclear, but incorrect: we simply take the retrieved state vector from the retrieval that minimises the errors in DWR. This is now explained in the text.

> We carry out a pseudo-retrieval by running multiple $Z_{10,35,95}\,V_{35}$ retrievals in which ~~PSD shape is assumed to take~~ the PSD shape parameter takes integer values from $\mu = -2$ to $\mu = 10$. The ~~pseudo-retrieval is made by selecting the value of PSD shape that~~ retrieved value is that which minimises the error in forward-modelled DWR_{35-95} and DWR_{10-35} between 400 and 600 m above ground level (Fig. 10a & b)~~; the state vector is linearly interpolating between the retrieved state vectors at the retrieved value~~. The forward-modelled DWRs for a range of PSD shape ~~, giving an estimate of the other retrieved quantities when the PSD shape is retrieved (Fig. 10~~parameters span up to 4 ~~d–g).~~ dB, with the range depending on the median volume diameter. To reduce noise in the pseudo-retrieval the minimisation is carried out at a smoothed temporal resolution of 15 s.

Technical Corrections:

Thank you for your thorough reading. We have gratefully made all of the suggested changes.

P1 L1: "cloud" should be "clouds"

P2 L26; P12 L8; P12 L20: "remote-sensed" should be "remotely-sensed"

P2 L26-L28: This sentence should be modified to be, "... in-situ measurements of snow events (Kneifel et al., 2015), but more detail of how the parameters... remains to be explored."

P2 L31-L32: No hyphens are needed between the frequency and unit as they are not acting as compound descriptors in this context. 95 should also have a 'GHz' after it, and I'd add a comma after "35 GHz".

P3 L10-13: These sentences should be reworked avoid three separate clauses strung together with semicolons. Consider making the third clause its own sentence.

P4 L16: "in" should be "as".

P6 L6: "95-GHz" should be "95 GHz".

P6 L20: "assumptions to" should be "assumptions of".

P7 L8: "(Kneifel et al., 2015)" should be "Kneifel et al. (2015)".

P7 L25: I believe this semicolon should be a comma.

P9 L14-L15: I would be consistent and just refer to "the ratios between radar backscatter cross-sections at 10-35-GHz and 35-95-GHz" as the DWR10-35 and DWR35-95 as already done in the text. This applies to the legend and caption of Figure 2 as well.

P16 L27: "The retrieved timeseries of PSD..." should be "The retrieved timeseries of PSD shape..."

P16 L29: "...the retrieved PSD noisy..." should be "... the retrieved PSD shape [factor] is noisy..."

P17 L24: "mixed-phase cloud" should be "mixed-phase clouds".

P17 L25: Should "distribution" be "relation"?

P18 L5: A space is needed after "surface".

P19 L1: "case comprised compact graupel..." should be "case was comprised of compact graupel..."

Referee #2

Specific comments:

The greatest concern is about the representativeness of the measurements obtained from the 10 minutes of rimed and 15 minutes of aggregated snow from the case study. This may not be sufficient to draw generalized conclusions about how this approach and overall novel methodology works. Slightly different environmental conditions could potentially produce altered results. The recommendation is to increase the number of cases for your radar analysis, perhaps 4-5 should suffice. Measurements from different geographical/climatological regions could also help to solidify your findings. If there is not much difference between the updated and the findings from the current version of the manuscript, add few paragraphs and/or table describing the statistics of the new dataset and retain the rest of the current analysis. If large discrepancies occur, the suggestion is to present a case with the statistics close to the one obtained from all available measurements. In this way, the generalization of the results would be justified.

As addressed in our general comments above, unfortunately a further 4 or 5 suitable snow events were not measured during BAECC 2014, but we have expanded the study to include a second, longer case study in which the snowfall differs significantly from the 21 February case. We take the broader point that our results for these case studies are not necessarily generalizable: the two contrasting case studies help to demonstrate this, and we have substantially re-written our discussion and conclusions to better represent the remaining uncertainties.

Technical corrections

We have gratefully made the following changes:

P7 L8: (Kneifel et al., 2015) should be Kneifel et al. (2015)

Figure 4: Add the temperature contours to the image if available.

Figure 9: "PSD shape μ" should be "PSD shape parameter μ"

P21 L10-14: This sentence is a bit hard to follow, perhaps split it in two.

Referee #3

General comments

Why do you use the mean Doppler velocity at 35 GHz in the retrieval? I was unable to find why this frequency is optimal for the retrieval methodology. Please add some information.

We now note in both Section 2.2 and in the case study and retrieval (Section 4) that the 95 GHz radar had a mispointing error during BAECC 2014 that makes it difficult to use the mean Doppler velocity. We therefore use the Doppler velocity from the most sensitive available instrument, the 35 GHz. In practice for snow near the surface, the 10 GHz mean Doppler velocity could also have been used.

PIP PSDs and other products are available at 1 min resolution. Why do you choose 5 min? If it is for better statistics through averaging, please make that point. Also, if you are using these values during the 25 minutes of the event, this essentially leaves 5 points for comparison with the retrieval. Could you expand on why you feel this is enough in situ data for assessment of aspects of the retrieval?

We are not using the PIP data directly, but rather the retrieval of von Lerber et al. (2016), which includes an estimate of the snow bulk density. This method requires a sufficient sample of ice particles, hence the use of a 5 minute resolution. We have now added this explanation to Section 2.2:

In situ measurements of ~~the~~ snow at the surface are provided by the Particle Imaging Package (PIP) video disdrometer [*Newman et al.*, 2009]. ~~PIP measurements and retrievals~~ While the temporal resolution of PIP measurements is 1 minute, estimates of parameters of the PSD and ~~bulk particle density at~~ particle properties are made over 5 minute ~~temporal resolution from Hyytiälä are described in *Tiira et* al. [2016]~~ intervals in order to increase the statistical sampling during BAEC while still resolving changes in the properties of snowfall at the surface, as described in *von Lerber et* al. [2017] [also *Moisseev et al.*, 2017; ~~*von Lerber et* al., 2017~~ *Tiira et* al., 2016]. The method of moments is used to estimate the parameters of the Gamma distribution from the measured PSD [*Moisseev and Chandrasekar*, 2007].

How did the prefrontal versus frontal period get defined? Is it purely from radar features? Maybe something more rigorous or not from the radar would be more appropriate (since you are using the radar to evaluate the method). Is there collocated met equipment that can be used to determine the onset of the front? You have collocated radiosondes – are those used to determine the timing of the front? Or maybe could help justify the time chosen.

We agree that the definition of the front was not clear, and in fact was probably not necessary to make the analysis, which is more focused on comparing the rimed and unrimed snow. We now refer to the two regimes in this case as "rimed" and "unrimed", rather than "prefrontal" and "frontal", based on the transition in radar and particle imaging measurements (Figs. 6 & 7).

Since one event is being used to test the efficacy of this method, I think this needs to be emphasized. Also, would be good to argue why this one event may be applicable to other similar particles or events in different locations.

We agree. We now more strongly stress that the limited cases from BAECC 2014 help to demonstrate the effects of the PSD shape parameter and internal structure of aggregates on triple-frequency radar measurements, but that longer and more diverse measurements are needed to better understand their relative importance to global snowfall.

Specific comments

Unless responded to directly, we have appreciatively made the following changes.

Page 2, Lines 7 – 11: Split into two sentences

Page 2, Lines 26 – 27: "but it remains to explore..." does not make sense

Page 2, Line 31: Be consistent with your "-" or not for frequencies (either all should be 35-GHz or should be 35 GHz

Page 3, Line 12: replace the "measurements;" with "measurements."

Page 3, Line 14: "advantages" should be "advantage"

Page 4, Line 1: Define CAPTIVATE

Page 4, Line 23: Make mass-size equation on own line with equation number

Page 4, Line 27: "AR" should be in parentheses. Also, the author goes between saying AR, axial ratio, and aspect ratio throughout the document. Be consistent (I recommend "AR" since you define it)

Page 5, Line 5: Should measurement vectors be numbered as well?

Page 7, Line 28: aspect ratio "AR"

Page 7, Line 34: "The range of radar signatures is overlaid with the measured triple-frequency radar data from Hyytiälä..." You already talk about the shape of the data (the hook feature) earlier. I think you should introduce the overlaying of this data before getting into the description above.

In response to this and other comments, we have removed the overlaid radar measurements from these figures (as well as adding a second kind of aggregate snowflake model). This makes the main focus of this figure the sensitivity to the different parameters, and also shows more clearly the fit to observations when we show the case studies. The discussion has been modified accordingly, and is hopefully now more linear.

Page 9, Line 2: 3mm for the spheroids but maybe more like 4mm for the fractal particles?

We now just say "around 3mm".

Page 9, Lines 10 - 11: Reference needed.

This was the result shown in the figure. To better link the earlier result, we now write,

> We have shown that, based on simulated radar backscatter cross-sections, the PSD shape parameter has a greater influence on the simulated triple-frequency radar signature than the well-known effect of particle density.

Page 9, Line 34: "We may therefore..."

Page 12, Lines 3 - 5: Please add some details about the frontal passage – i.e., met data or observations that are not radar or particle focused. This will justify better your distinction of the two regimes (since you are using radar and in situ particle obs to test and assess the retrieval).

As stated above: we have chosen to de-emphasise the frontal passage in this case, as it is not strictly necessary for interrogating the snow microphysics. We have added a reference to the more detailed dicussion in Kneifel et al. 2015.

Page 12, Lines 20 - 22: Reference needed

Page 14, Lines 2 - 3: "...suggesting that some rimed particles persist after 23:03 UTC." Could it be the choice of timing of the prefrontal versus frontal is off? Would using collocated met data clarify this?

As discussed earlier, we now simply distinguish between rimed and unrimed snow regimes. In this context, it doesn't seem especially problematic that there would be a mixture of rimed and unrimed snow in the transition between the regimes.

Page 14, Line 7: "...in situ measurements at the surface." Please specify what this is from—I assume the PIP measurements?

Page 18, Lines 12 —13: I do not understand "A significant difference between the frontal and the prefrontal profiles is that all retrievals are able to represent the observed profile of mean Doppler velocity below about 1.5 km," as I am not see this. Could you please add some details as to what you are referring?

We agree that this was unclear. This sentence now reads,

> A significant difference between the ~~frontal and the prefrontal~~ profiles is that ~~all retrievals~~ in the unrimed regime retrievals that do not assimilate Doppler velocity are able to represent the observed profile of mean Doppler velocity~~below about 1.5 km, showing that the prior density factor of~~ : this is because the a priori density factor ($r = 0$~~makes an accurate~~) makes a reasonable estimate of the terminal fallspeed of unrimed aggregate particles, provided that their size is well-constrained by dual-frequency radar ~~measurements – even when mean Doppler velocity measurements are not assimilated.~~

Page 19, Lines 9 – 11: The truncation you refer to here – are you talking about the PIP or the method? Both have lower limits. And technically snow is always dominated by small particles – just less so or more so depending on the shape of the PSD. So I do not think this is the correct sentiment here (i.e., even when a PSD is quite broad with lots of large aggregates, there still tends to be 1 to 2 orders of magnitude more small particles. When the PSD is quite narrow that is more like a factor of 3 to 4 orders of mag... but still lots of small particles in a broad distribution).

We now cite Moisseev and Chandresekhar (2007) regarding the effects of disdrometer truncation on the method of moments.

Pages 19 – 23: This section almost feels a bit out of order. It is like there are conclusions at the beginning and the discussion of application shown in Fig. 9 further into the section. It may help potential readers to move the discussion of the Fig. 9 to earlier in this section and move the verbiage in the beginning of the section to later – as a transition to conclusions.

Thank you for this—we agree, and hope that the discussion and conclusions have benefited from a significant re-write. We have opted to remove Fig.9 after introducing additional figures for the second case study, while still briefly discussing that it is unknown how closely related the PSD shape parameter is with riming. Hopefully the flow of the discussion and conclusions is now clearer and more concise.

The importance of particle size distribution ~~shape~~ and internal structure for triple-frequency radar retrievals of the morphology of snow

Shannon L. Mason[1,2], Robin J. Hogan[3,1], Christopher D. Westbrook[1], Stefan Kneifel[4], Dmitri Moisseev[5,6], and Leonie von Terzi[4]

[1]University of Reading, Reading, UK
[2]National Centre for Earth Observation, Reading, UK
[3]European Centre for Medium-range Weather Forecasts, Reading, UK
[4]University of Cologne, Cologne, Germany
[5]University of Helsinki, Helsinki, Finland
[6]Finnish Meteorological Institute, Helsinki, Finland

Correspondence: Shannon L. Mason (s.l.mason@reading.ac.uk)

Abstract. The accurate representation of ice particles is essential for both remotely-sensed estimates of ~~cloud~~ clouds and precipitation and numerical models of the atmosphere. As it is typical in radar retrievals to assume that all snow is composed of ~~unrimed~~ aggregate snowflakes, both denser rimed snow and the mixed-phase cloud in which riming occurs may be under-diagnosed in retrievals, and therefore difficult to evaluate in weather and climate models. Recent experimental and numerical studies have yielded methods for using triple-frequency radar measurements to ~~distinguish fractal aggregate snowflakesfrom~~ interrogate the internal structure of aggregate snowflakes, and to distinguish more dense and homogeneous rimed particles from aggregates.

In this study we investigate which parameters of the ~~particle size distribution (PSD) and morphology~~ morphology and size distribution of ice particles ~~are most important to~~ most affect the triple-frequency radar signature ~~of snow,~~ and must therefore be accounted for in order to carry out ~~an optimal estimation retrieval using~~ triple-frequency ~~Doppler radar observations. We represent a~~ radar retrievals of snow. A range of ice particle morphologies are represented, using a fractal ~~model for aggregate snowflakes~~ representation for the internal structure of aggregate snowflakes, and homogeneous spheroids to represent ~~rimed~~ graupel-like particles~~, and modulate the prefactor and exponent of the particles' mass-size relations with~~ ; the mass- and area-size relations are modulated by a density factor. We find that ~~for both fractal particles and homogeneous spheroids~~ the PSD shape ~~has a greater influence on the~~ parameter and the parameters controlling the internal structure of aggregate snowflakes both have significant influences of triple-frequency radar signature~~than the density factor, and show that the PSD shape must~~ , and are at least as important as that of the density factor. We explore how these parameters may be allowed to vary ~~to adequately constrain a~~ in order to prevent triple-frequency radar ~~retrieval of snow . We then demonstrate a novel triple-frequency Doppler radar retrieval of three parameters of the PSD as well as particle density, and show that the estimated snow rate, PSD and bulk density compare well against in situ observations at the surface~~retrievals of snow from being over-constrained, using two case studies from the Biogenic Aerosols—Effects of Clouds and Climate (BAECC) 2014 field campaign at Hyytiälä, Finland. In a

case ~~study of compact rimed snow , we find~~ including heavily rimed snow followed by large aggregate snowflakes, we show that triple-frequency radar measurements provide a strong constraint on the ~~estimation of PSD shape , but a relatively weak constraint on particle density, which we find can be more directly estimated from the Doppler velocity~~ PSD shape parameter, which can be estimated from an ensemble of retrievals; however, resolving variations in the PSD shape parameter has a limited impact on estimates of snowfall rate from radar. Particle density is more effectively constrained by the Doppler velocity than triple-frequency radar measurements, due to the ~~relation between particle density and fallspeed . Including variations in PSD shape as well as particle morphology allows for a better representation of the~~ strong dependence of particle fallspeed on density. Due to the characteristic signatures of aggregate snowflakes, a third radar frequency is essential to effectively constraining the size of large aggregates. In a case featuring rime splintering, differences in the internal structures of aggregate snowflakes are revealed in the triple-frequency ~~radar signatures of rimed and unrimed snow, and suggests the potential for making new insights into the interaction between particles during aggregation and riming mechanisms. However, we find that improved representation of the PSD shape has a limited impact on improved estimates~~ radar measurements. We compare retrievals assuming different aggregate snowflake models against in situ measurements at the surface, and show significant uncertainties in radar retrievals of snow rate ~~from radar~~due to changes in the internal structure of aggregates. The importance of the PSD shape parameter and snowflake internal structure to triple-frequency radar retrievals of snow ~~suggests that further work is needed to account for variations in PSD shape~~ highlights that the processes by which ice particles interact may need to be better understood and parameterised before triple-frequency radar measurements can be used to ~~better constrain~~ constrain retrievals of ice particle morphology.

1 Introduction

Remotely-sensed estimates of ice clouds and snow from spaceborne radars inform our understanding of key components of the global water and energy cycles. Both retrieval algorithms and numerical weather and climate models rely on a representation of the ice particle size distribution (PSD) and morphology, which are functions of the microphysical processes by which ice particles form, interact and grow. The processes of deposition, aggregation and riming may all contribute to the formation of a snowflake, and this growth history is encoded in the morphology of an ice particle. As riming requires the interaction of precipitating ice with supercooled liquid droplets in mixed-phase cloud layers which are difficult to diagnose, it has long been assumed that the majority of snow falls as unrimed ~~pristine or~~ aggregate snowflakes [*Langleben*, 1954]~~; however~~. However, recent global active remote-sensing suggests that mixed-phase clouds are frequently associated with snow, especially over the ocean [*Battaglia and Delanoë*, 2013]. Nevertheless, it has been typical to assume a fixed representation of the morphology and size distribution of ice particles, usually derived from measurements of unrimed aggregates [e.g. *Delanoë*, 2008; *Hogan et al.*, 2012]. This means that many radar retrievals of snow do not represent particles which have grown by riming, a process which

can contribute a significant fraction of the mass of snow [*Mosimann*, 1995; *Grazioli et al.*, 2015; *Tiira et al.*, 2016; *Moisseev et al.*, 2017; *von Lerber et al.*, 2017].

Radar retrievals that allow variation in the morphology of ice particles are therefore of significant interest, and the development of novel retrieval methods has been facilitated by measurement campaigns combining multiple-frequency radars and other remote-sensing instruments with in situ measurements of snow particle properties [e.g. *Szyrmer and Zawadzki*, 2014a; *Petä*, 2016]. Doppler velocity measurements of ~~the terminal fallspeed of~~ snow have been used to constrain variations in particle density by which riming~~of snow~~, and the mixed-phase cloud in which it occurs, can be diagnosed [*Mosimann*, 1995; *Szyrmer and Zawadzki*, 2014a, b; *Mason et al.*, 2018]. Variations in the density of ice particles are also related to changes in their shape and structure—whether due to aggregation, riming or a combination of processes—which are reflected in their radar backscatter cross-sections [*Leinonen and Szyrmer*, 2015]. *Mason et al.* [2018] formulated a single parameter modulating the density, shape and structure of ice particles, which was retrieved in single- and dual-frequency Doppler radar retrievals, and was chiefly constrained by the mean Doppler velocity. This representation was based on a large database of ice particle mass- and area-size relations and insights from ~~remote-sensed~~ remotely-sensed and in-situ measurements of snow events [*Kneifel et al.*, 2015], but ~~it remains to explore in more detail~~ how the parameters controlling the size distribution and morphology of snow particles relate to one another and their radar scattering characteristics is not yet fully understood.

The relation between ice particle morphology and triple-frequency radar measurements emerges in a comparison of models for the radar backscatter cross-sections of ice particles [*Kneifel et al.*, 2011]. The triple-frequency radar 'signature' consists of radar measurements at three frequencies spanning the millimeter wavelength range, the two dual-wavelength ratios (DWRs) ~~derived from radar measurements~~ of which reveal information about non-Rayleigh scattering from larger snowflakes. Typically radars at 95, ~~35 GHz~~ 35 and a third frequency ~~below 15 GHz, and provides~~ between 3 and 15 GHz are used [e.g. *Kneifel et* al., 2015; *Leinonen and Szyrmer*, 2015; *Barrett et* al., 2019]. The triple-frequency radar signature has provided a succinct means of evaluating the applicability of spheroidal particles as models for fractal aggregate snowflakes [*Leinonen et al.*, 2012], revealing the fractal dimension of observed aggregates [*Stein et al.*, 2015], and exploring their microphysical structure [*Leinonen and Moisseev*, 2015]. Triple-frequency radar observations of rimed snow combining ground-based radar and in situ measurements [*Kneifel et al.*, 2015] showed the apparent influence of increasing particle density on the triple-frequency radar signature, while a modelling study of the combined effects of growth by aggregation and riming related triple-frequency measurements to microphysical processes [*Leinonen and Szyrmer*, 2015]. Combining triple-frequency and Doppler velocity information, *Kneifel et al.* [2016] used triple-frequency Doppler spectra to identify the spectral signatures of rimed and unrimed snow. The insights provided by triple-frequency radar techniques have contributed to the development of expanded scattering databases for representing and evaluating a wide range of ice particles [*Kneifel et al.*, 2018].

The strong numerical and observational evidence that the triple-frequency radar signature reflects the density and structure of snow particles suggests the potential for retrievals in which some morphological parameters are constrained by triple-frequency radar measurements. Triple-frequency radar retrievals have been demonstrated in which the structure and density of ice particles are allowed to vary, but where the PSD Shape is assumed constant [~~*Leinonen et* al., 2018~~*Leinonen et* al., 2018a; *Tridon et al.*, 2019]; however, it is not yet clear which ~~ice particle properties~~ properties of ice particle are best constrained by the triple-

frequency radar measurements~~; *Leinonen et* al. [2018]~~ . *Leinonen et* al. [2018a] found that a triple-frequency radar retrieval of the mass-size relation of ice particles did not differ significantly from that of a dual-frequency retrieval, suggesting that the problem is over-constrained. It has been shown that the higher-order moments of the Doppler spectra from multiple-frequency radars can be used to reduce the uncertainty of retrievals of ice clouds [*Maahn and Lö*, 2017]; however, triple-frequency radar signatures are most distinct for larger precipitating particles. To our knowledge ~~, a~~ a retrieval assimilating both triple-frequency ~~Doppler retrieval of ice~~ radar reflectivity factors and mean Doppler velocity to estimate the properties of snow has not yet been ~~described—this may~~ described. This approach should have the advantages of ~~estimating particle density constrained by~~ constraining particle density with Doppler velocity [as in *Mason et al.*, 2018]~~and~~ , while using triple-frequency radar signatures to constrain some ~~parameters of particle morphology~~additional parameter affecting the microphysical properties or size distribution of precipitating ice particles.

In this study we explore the potential for a triple-frequency Doppler radar retrieval using the optimal estimation framework Cloud Aerosol and Precipitation from mulTiple Instruments using a VAriational TEchnique [CAPTIVATE; *Mason et al.*, 2018]. In Section 2 we briefly describe the key components of the radar forward-model, and the remotely-sensed and in situ data used to perform and evaluate the retrieval. In Section 3 we ~~then explore the effects of ice~~ explore how parameters controlling the PSD and particle ~~morphology parameters on~~ properties affect the forward-modelled triple-frequency radar signatures of ~~fractal and homogeneous spheroid models for~~ aggregate snowflakes and graupel-like particles~~, respectively. In Section ?? we compare our models for snow particles against~~ . We then apply these insights to triple-frequency radar measurements from ~~a case study of rimed and unrimed snow during~~ the Biogenic Aerosols—Effects of Clouds and Climate (BAECC) field campaign in Hyytiälä, Finland in 2014 [*Petä*, 2016]. In Section 4 we use our particle models to represent the triple-frequency radar signatures of rimed and unrimed snow regimes based on their structure, density and PSD shape parameter. We demonstrate a triple-frequency Doppler radar retrieval ~~in the rimed and unrimed snow in which key parameters~~ of the PSD shape parameter and particle morphology~~are retrieved~~, and evaluate ~~the~~ remotely-sensed estimates against in situ measurements at the surface. In Section ~~??~~ ~~we summarise our findings and make some concluding remarks~~5 we consider the triple-frequency radar signatures from a case study featuring secondary ice production due to rime splintering, with a focus on the presence of large aggregates with distinct triple-frequency radar signatures. Finally, we summarise our conclusions in Section 6.

2 Methods and data

We first describe the ~~retrieved state variables and radar measurement variables~~ state and observation variables in the retrieval framework (Section 2.1), then outline the radar measurements assimilated into the retrieval and in situ measurements against which the retrieval is evaluated (Section 2.2).

2.1 Radar forward model and retrieval algorithm

We use the optimal estimation retrieval algorithm ~~CAPTIVATE~~ Cloud Aerosol and Precipitation from Multiple Instruments using a Variational Technique (CAPTIVATE) described by *Mason et al.* [2018]. This framework has been developed for re-

trievals with the Doppler cloud profiling radar aboard EarthCARE [*Illingworth et al.*, 2015], but is configurable for multiple radar instruments in ground-based and airborne, as well as spaceborne, applications. Here we describe the major components of the CAPTIVATE radar forward-model pertinent to ice and snow.

The ice PSD is given by

$$N(D) = N_w F(D/D_0, \mu), \tag{1}$$

where N is the number of particles ~~N~~ of maximum dimension D, ~~represented by the normalized gamma distribution~~

~~$$N(D) = N_w \frac{\Gamma(4)}{4^4} \frac{(4+\mu)^{4+\mu}}{\Gamma(4+\mu)} \frac{D}{D_0} \exp\left(-(4+\mu)\frac{D}{D_0}\right),$$~~

~~where~~ N_w is the normalized number concentration, ~~D_0 is the median volume diameter, Γ is the gamma function, and μ the shape parameter of the PSD~~ and F is the normalized gamma distribution [*Testud et al.*, 2001; *Illingworth and Blackman*, 2002; *Delanoë*, 2005]~~. While the majority of triple-frequency radar studies thus far have assumed the exponential PSD (i.e. $\mu = 0$) , in situ measurements of snow at Hyytiälä include Gamma PSD shapes in the range $-2 < \mu < 5$ Fig. 15 in *Tiira et* al., 2016.~~ , which is a function of the median volume diameter (D_0) and the shape parameter of the PSD (μ). Modified 'universal' PSDs formulated to address the need for non-exponential distributions in ice clouds [*Delanoë*, 2005; *Field et al.*, 2005, 2007] ~~have been~~ are also implemented in CAPTIVATE [*Mason et al.*, 2018]~~; however,~~ , but in this study Gamma PSDs are used in order to explore the effects of accounting for PSDs broader ($\mu < 0$) and narrower ($\mu > 0$) than the exponential. While the majority of triple-frequency radar studies assume an exponential PSD (i.e. $\mu = 0$), in situ measurements of snow at Hyytiälä suggest Gamma PSD shape parameters vary in the range $-2 < \mu < 5$ [Fig. 15 in *Tiira et* al., 2016].

The morphology of ~~the~~ ice particles is represented by ~~three~~ parameters controlling their microphysical structure, density, and shape. ~~The microphysical structure is represented in an approximation to~~ Approximations to the microphysical structure of ice particles are used to calculate the radar backscatter cross-section ~~$\sigma(D)$~~ (σ) of each particle. ~~In this study we use two approximations~~ We use two methods to represent the range of particle structures from aggregates snowflakes to graupel. ~~Aggregate snowflakes are represented as fractal particles using the~~ The scattering cross-section of low density particles such as aggregates can be represented using the Rayleigh-Gans approximation, wherein the interactions between dipoles within the particle are neglected, and the electric field experience by each dipole is equal to the incident field. In the Self-Similar Rayleigh Gans Approximation [SSRGA; *Hogan and Westbrook*, 2014; *Hogan et al.*, 2017] ~~after the aggregate snowflake~~ the radar backscatter cross-section of a low-density particle deviates from Rayleigh scattering according to

$$\phi_{\mathrm{SSRGA}}(kD) = \frac{\pi^2}{4}\left(\cos^2(kD)A(kD,\kappa) + \sin^2(kD)\sum_{j=1}^{n} B(j,\zeta,\beta,\gamma)\right), \tag{2}$$

where $k = 2\pi/\lambda$ is the wavenumber at radar wavelength λ and D the maximum dimension of the particle. The effect of the average particle geometry A is a function of the kurtosis κ of the distribution of mass about the centre of the particle. The effect of the internal structure is given by the integral over a power spectrum representing random fluctuations about the

average particle geometry,

$$B = \beta\zeta_j(2j)^{-\gamma}\left[\frac{1}{(2kD+2\pi j)^2}+\frac{1}{(2kD-2\pi j)^2}\right] \quad (3)$$

where j is the index of the wavenumber. The power law prefactor β represents the amplitude of fluctuations about the average particle geometry, while the power law exponent γ controls the relative importance of fluctuations at small scales. The scaling factor ζ_j was introduced in *Hogan et* al. [2017] to reduce the amplitude of the internal structure at the largest scale (i.e. $\zeta_1 \leq 1$, then $\zeta_j = 1$ for $j > 1$).

A fit to aggregates of bullet rosettes from the aggregation model of *Westbrook et al.* [2004] ~~. Heavily rimed graupel-like~~ was derived by *Hogan et* al. [2017]. Based on the observation that aggregates of most monomers (e.g. dendrites, plates and columns) had similar statistics, this model has been applied to CAPTIVATE retrievals of aggregate snowfall [e.g. *Mason et* al., 2018]; however, in Section 3 we will also consider the effect of variations in snowflake structure on the triple-frequency radar signature. As the Rayleigh-Gans approximation applies to low-density particles in which the interactions between dipoles can be neglected, denser heavily rimed aggregates and graupel particles are represented using the T-matrix approximation ~~for~~ to 'soft spheroids' composed of ~~a homogeneous mixture~~ homogeneous mixtures of ice and air [e.g. *Hogan et al.*, 2012]. This ~~approximation is not suited to representing aggregate snowflakes, but~~ provides a good approximation to graupel, but is known to under-estimate the backscatter from aggregate snowflakes [*Leinonen and Szyrmer*, 2015].

The density factor r ~~is a parameterisation described by *Mason et* al. [2018], which~~ varies both the prefactor and exponent of the ice particle mass-size relation ~~$m(D) = aD^b$,~~

$$m(D) = aD^b \quad (4)$$

between that of the "aggregates of unrimed bullets, columns and side-planes" of *Brown and Francis* [1995] at $r = 0$, and that of spheroids of solid ice at $r = 1$. *Mason et al.* [2018] showed that this parameter allowed for simplified representation of a broad range of measured mass-size relations for particles along a continuum from unrimed aggregates to rimed snow, graupel, and hail. Finally, the volumetric shape of all particles is defined by ~~horizontally-aligned oblate spheroids with axial ratio~~ the axial ratio (AR) of horizontally-aligned oblate spheroids.

We note that in nature the structure, density and shape of snow particles are not independent. As discussed in ~~more detail in~~ *Mason et al.* [2018], the fractal or homogeneous distribution of mass through the volume of a particle is closely related to its density: the fractal structure of aggregates snowflakes is characterised by a mass-size relation with an exponent close to $b = 2$, while more homogeneous graupel and hail particles have mass-size relations with b approaching 3. The riming process by which aggregates accrete mass to become more graupel-like is also known to change the particle shape, with axial ratios increasing from more oblate snowflakes ($AR \approx 0.6$) to rounder graupel particles ~~with~~ ($AR > 0.8$) [*Li et al.*, 2018].

2.1.1 State vector

As described in *Mason et al.* [2018], CAPTIVATE has been developed for radar-lidar-radiometer synergy from the upcoming EarthCARE satellite, and the retrieval of ice and snow follows the work of *Delanoë* [2008] for radar-lidar synergy. The state

vector ~~is:~~

$$\mathbf{x} = \begin{pmatrix} \ln \alpha_\mathrm{v} \\ \ln N_0' \\ r' \end{pmatrix},$$

~~where the~~ for a vertical profile is:

$$\mathbf{x} = \begin{pmatrix} \boldsymbol{\ln \alpha_\mathrm{v}} \\ \boldsymbol{\ln N_0'} \\ \boldsymbol{r'} \end{pmatrix}, \tag{5}$$

where the state variables, the visible extinction coefficient α_v in the geometric optics approximation and the primed number concentration N_0', are chosen so that prior ~~estimate~~ estimates can be made as a function of atmospheric temperature [see Fig. 3 of *Delanoë*, 2008]. Retrieving both of these terms provides sufficient degrees of freedom to derive two parameters of the PSD, the median volume diameter and normalized number concentration; these more physically meaningful values, rather than the state variables, are reported in this study. The natural logarithms of most parameters are used to avoid non-physical negative values and to improve convergence~~, while~~. The final state variable is the density index r'~~state variable is~~, a function of the density factor such that r' is defined at all real values [*Mason et al.*, 2018]. To reduce the effect of measurement noise on the retrieval, the retrieved state variables through the vertical profile are represented as the basis functions of a cubic spline [*Hogan*, 2007]. The PSD shape ~~, ice particle~~ parameter, axial ratio and chosen ~~model for ice particle structure and radar backscatter~~ radar backscatter approximation are configurable at runtime, but are assumed constant within each retrieval.

2.1.2 Measurement vector

The radar reflectivity factor ~~(in linear units)~~ at frequency f is given (in linear units) by

$$Z_f = \frac{\lambda_f^4}{\pi^5 |K_w|^2} \int_0^\infty \sigma_f(D)\, N(D)\, dD \tag{6}$$

where λ_f is the radar wavelength, K_w is the dielectric factor of water at cm wavelengths, and $\sigma_f(D)$ is the backscatter cross-section for a particle of maximum dimension D at the radar frequency. The dual-wavelength ratio (DWR) between frequencies f_1 and f_2 is then $\mathrm{DWR}_{f_1-f_2} = Z_{f_1}/Z_{f_2}$. Both radar reflectivity and DWR are reported in dB unless otherwise stated. While DWR quantities are reported here, the radar reflectivity factors at each frequency are used in the measurement vector.

Mean Doppler velocity is given by

$$V_f = \frac{\int_0^\infty v(D)\, \sigma_f(D)\, N(D)\, dD}{\int_0^\infty \sigma_f(D)\, N(D)\, dD}, \tag{7}$$

where the terminal velocity of an ice particle $v(D)$ assumes negligible vertical air motion, and positive values of mean Doppler velocity are toward the surface.

The measurement vector for n radar frequencies is therefore given by

$$\mathbf{y} = \begin{pmatrix} Z_{\mathrm{f}_1} \\ \vdots \\ Z_{\mathrm{f}_n} \\ V_{\mathrm{f}_1} \\ \vdots \\ V_{\mathrm{f}_n} \end{pmatrix}.$$

~~In practice we may also~~

$$\mathbf{y} = \begin{pmatrix} Z_{\mathrm{f}_1} \\ \vdots \\ Z_{\mathrm{f}_n} \\ V_{\mathrm{f}_1} \\ \vdots \\ V_{\mathrm{f}_n} \end{pmatrix}. \tag{8}$$

In this paper we perform retrievals using two or three radar frequencies, and use mean Doppler velocity at one radar frequency.

2.2 Radar and in situ measurements

Atmospheric Radiation Measurement second mobile facility (AMF2) Doppler radars at 10, 35 and ~~95-GHz~~ 95 GHz were deployed at Hyytiälä, Finland during the ~~Biogenic Aerosols—Effects on Clouds and Climate (BAECC) field campaign in 2014~~ BAECC 2014 field campaign [*Petä*, 2016]. Radar measurements used here are at ~2 s temporal and ~30 m vertical resolution, and radar ~~reflectivities~~ reflectivity factors have been corrected for gaseous and liquid attenuation. The specifications of the AMF2 radars, and their colocation, calibration and attenuation correction for triple-frequency radar measurements during BAECC 2014 are described in *Kneifel et al.* [2015]. Due to a mispointing of the 95 GHz radar during BAECC, the mean Doppler velocity for that radar is not used in this study.

In situ measurements of ~~the~~ snow at the surface are provided by the Particle Imaging Package (PIP) video disdrometer [*Newman et al.*, 2009]. ~~PIP measurements and retrievals~~ While the temporal resolution of PIP measurements is 1 minute, estimates of parameters of the PSD and ~~bulk particle density at~~ particle properties are made over 5 minute ~~temporal resolution from Hyytiälä are described in *Tiira et* al. [2016]~~ intervals in order to increase the statistical sampling during BAEC while still resolving changes in the properties of snowfall at the surface, as described in *von Lerber et* al. [2017] [also *Moisseev et al.*, 2017; ~~*von Lerber et* al., 2017~~*Tiira et* al., 2016]. The method of moments is used to estimate the parameters of the Gamma distribution from the measured PSD [*Moisseev and Chandrasekar*, 2007].

~~The case study in Section ??~~ Due in part to the scanning strategy of the 35 and 10 GHz radars during BAECC, zenith-pointing measurements from all three radars coincident with sufficient snowfall measured by PIP at the surface were rare during

the observation period. The case studies consists of approximately 25 minutes of zenith-pointing triple-frequency Doppler radar data ~~from~~ between 22:53 ~~to~~ and 23:18 UTC on 21 February ~~2014. The radar~~ 2014 (Section 4), and one hour between 00:00 and 01:00 UTC on 16 February 2014 (Section 5). Radar measurements are complemented by ~~a radiosonde profile of atmospheric pressure, temperature and humidity which provides~~ contemporary radiosonde profiles and numerical weather prediction analyses which provide thermodynamic information for the retrieval.

3 ~~Influences on~~ Parameters affecting the triple-frequency radar signature

In this section we ~~use approximations to radar backscatter cross-section to explore the importance~~ explore the effects of ice particle morphology and size distribution on the triple-frequency radar signature. As described in Section 2.1~~.1, we represent ice particle morphology using parameters that control~~ , the representation of ice particles can be controlled by parameters for their microphysical structure, density and shape. ~~We consider the~~ Two approximations to the radar backscatter cross-section are used to represent the range of particle structures~~by comparing two approximations to radar backscatter cross-sections:~~ : low-density aggregate snowflakes are represented as fractal particles, ~~and heavily rimed~~ the complex internal of structures of which are controlled by the coefficients of a power law; while dense graupel-like particles are modelled as homogeneous spheroids. ~~The~~ For both fractal and homogeneous particles, the density factor and the axial ratio control the mass-size relation and ~~particle shape~~ the shape of the volume enclosing the particle. The final parameter is the PSD shape parameter, which is independent of ~~the particle morphology ,~~ particle morphology but affects the relative weighting given to particles across the size spectrum. Most studies of triple-frequency radar signatures of ice particles have assumed exponential PSDs [*Kneifel et al.*, 2011; *Leinonen et al.*, 2011; *Kneifel et al.*, 2015; *Leinonen and Moisseev*, 2015; *Leinonen and Szyrmer*, 2015].

~~For agiven particle morphology and PSD shape, the~~

We first consider the effect of variations in the internal structure of aggregates as represented in the SSRGA. In Figure 1 we show the sensitivity of the triple-frequency signature to the coefficients of the power spectrum representing the fluctuations about the average particle. Dual-wavelength ratios are enhanced by strong peaks in backscatter ratios at particle sizes where the radar backscatter is affected by constructive or destructive interference at one of the wavelengths (illustrated later in Fig. 4a). These spectral features are strongest in the radar backscatter cross-sections of soft spheroids [Fig. 9c of *Hogan et* al., 2017]. The SSRGA superimposes random smaller-scale structure onto the average particle structure, introducing random interference which smooths the resonant features over the spectrum, and reduces the maximum dual-wavelength ratios. The dual-wavelength ratios are reduced by either increasing the amplitude of the fluctuations (increasing the prefactor β), or by increasing the significance of structure at small scales (decreasing the exponent γ). Reducing the power law exponent to represent aggregates with a greater degree of structure at small scales also results in a more pronounced hook feature. Conversely, a power law exponent of $\gamma = 4$ is associated with the homogeneous distribution of mass at or below the scale of monomers in aggregates [*Hogan and Westbrook*, 2014]; the triple-frequency radar ~~signature represents the values of DWR_{35-95} and DWR_{10-35}~~ signatures at this limit, or where the amplitude of the fluctuations β approaches zero, come to resemble those of homogeneous spheroids with no hook feature (Fig. 2).

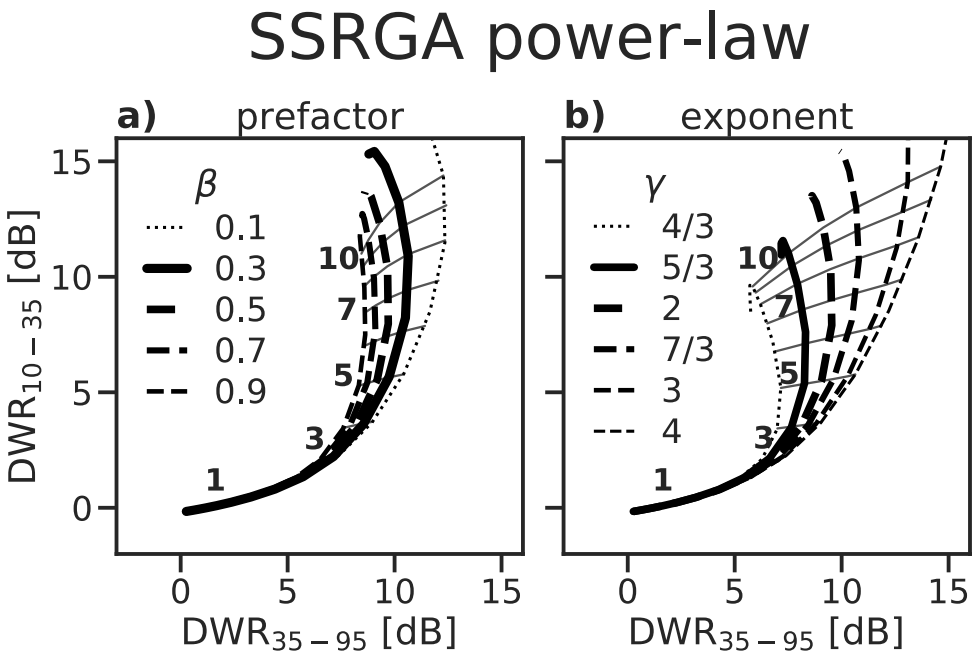

Figure 1. Forward-modelled triple frequency radar signatures for fractal particles represented by the SSRGA, with a range of values of (a) the power law prefactor β, where the exponent is constant ($\gamma = 2.0$); and (b) the power law exponent γ, where the prefactor is constant ($\beta = 0.55$). The other SSRGA parameters used are for the aggregates of bullet rosettes of *Hogan et* al. [2017], given in Table1. Lateral lines denote increments of median volume diameter, labelled in millimetres. All particles are assumed to have an exponential PSD ($\mu = 0$), a density factor of $r = 0$, and a particle axial ratio of $AR = 0.6$.

To identify the variability in these parameters for a range of ~~median volume diameters from 0.1~~aggregate snowflakes, we fit SSRGA parameters to simulated aggregates comprising a range of monomer types and size distributions. The various aggregates were generated using the aggregation code presented in *Leinonen and Moisseev* [2015], which assumes an inverse exponential distribution of monomer sizes from which the monomers are sampled. In total more than 30,000 aggregates of dendrite, plate, needle, and column monomers were generated covering maximum sizes up to 2 ~~to 20~~cm. For this, the characteristic size of the monomer distribution was varied from 0.2 to 1.0 mm~~. The~~ , with minimum monomer size of 0.1 mm and maximum size of 3 mm. Each aggregate consisted of up to 1000 monomers. SSRGA fits to aggregates of the range of monomers (Table 1) have similar characteristic triple-frequency ~~radar signatures for fractal particles~~ signatures (Fig. 2). The notable exception is aggregates of needles, for which the triple-frequency signature tends toward lower values of DWR_{35-95}, and the SSRGA power law exponent is lower, around $\gamma = 5/3$ rather than $\gamma \approx 2$. The power law prefactor for aggregates of needles denotes a relatively high degree of structure, with $\beta \approx 0.76$. These results are consistent with *Leinonen and Moisseev* [2015], who used the discrete dipole approximation to generate the triple-frequency radar signatures of a range of modelled aggregate particles and found that aggregates of large needles had characteristically lower values of DWR_{35-95} compared with aggregates

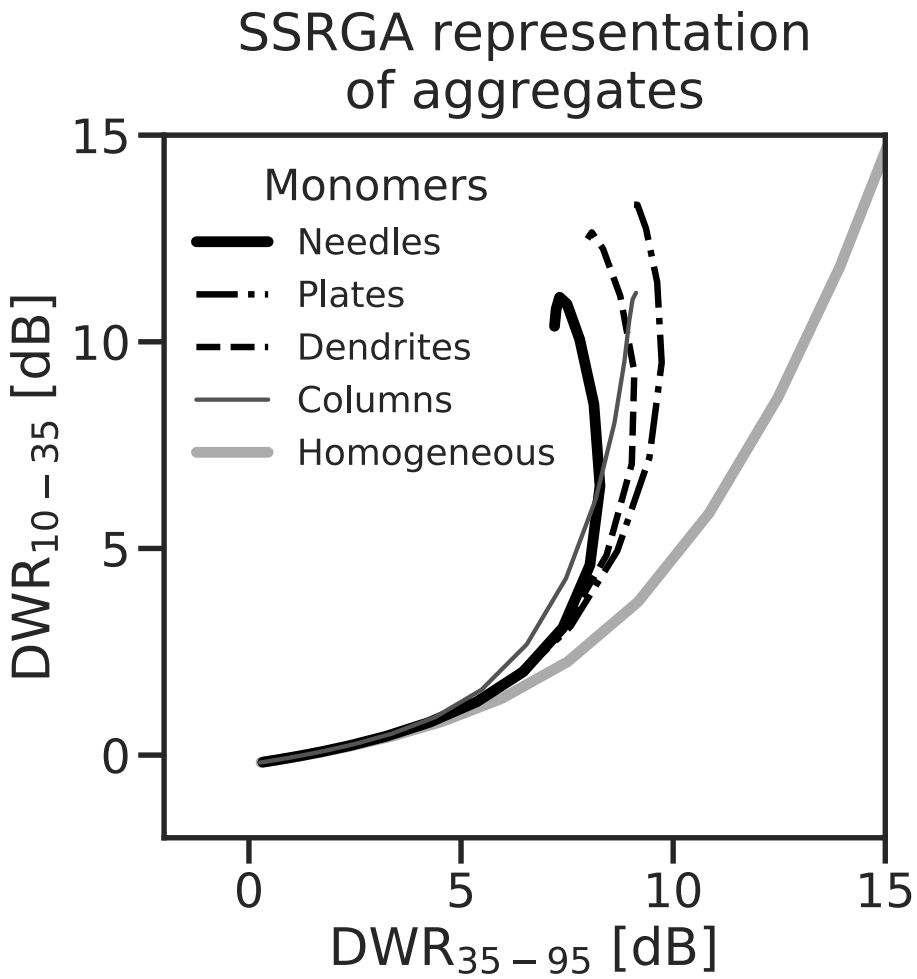

Figure 2. Triple-frequency radar signatures for SSRGA representations of four aggregates of different monomers (Table 1), and a representation of homogeneous particles ($\beta = 4$).

Monomer	κ	β	γ	ζ_1
Bullet rosettes [*Hogan et* al., 2017]	0.09	0.55	2.0	0.28
Plates	0.18	0.8	2.1	0.10
Dendrites	0.20	0.6	1.8	0.13
Columns	0.22	1.96	2.15	0.09
Needles	0.25	0.76	1.66	0.10

Table 1. SSRGA parameters fit to simulated aggregates of a range of monomers.

of other monomers. To encompass this range of triple-frequency radar signatures for aggregates, we employ SSRGA fits to two genres of fractal particles: aggregates of bullet rosettes to represent most snowflakes [*Hogan et* al., 2017]; and aggregates of needles.

Next we compare the triple-frequency radar signatures for aggregates of needles (Fig. 3 a–c), aggregates of bullet rosettes (Fig.3d–f), and homogeneous spheroids (Fig. 3 ~~d–f) are compared~~ g–i) for a range of values of ~~PSD shape (Fig. 3 a & d)~~the PSD shape parameter, density factor ~~, (Fig. 3 b & e) and aspect ratio(Fig. 3 c & f). Intervals of median volume diameter in millimeters are labeled in (Fig. 3 a & d). The~~ and axial ratio. Qualitatively, we note that the dual-wavelength ratios achieved by varying these parameters cover a similar range to the statistics of triple-frequency radar ~~signatures overlay triple-frequency radar measurements from the case study considered in more detail later (Section ??);~~ measurements [*~~Kneifel et~~* al., 2015*Dias Neto et* al., 20 ~~that these data reflect distinct triple-frequency signatures. The curved signatures with high values of DWR_{10-35} correspond to large aggregate snowflakes, and the flatter signatures with higher values of DWR_{35-95} to compact, heavily rimed snow.~~

~~Simulated triple-frequency radar signatures for distributions of (a–c) fractal particles represented using SSRGA and (d–f) homogeneous (“soft”) spheroids. Black lines illustrate radar signatures for a spectrum of PSDs with median volume diameters (values indicated in panels a and d) for different values of (a & d) PSD shape factor, (b & e) density factor, and (c & f) axial ratio. Lateral lines denote increments of median volume diameter in millimeters. Underlying the triple-frequency radar signatures are triple-frequency radar measurements from the 21 February 2014 case study at Hyytiälä, Finland *Kneifel et* al., 2015.~~

. The triple-frequency radar signatures for the fractal particles exhibit maxima in DWR_{35-95} between 8 and 12 dB for aggregates of bullet rosettes, and lower values around 7 to 8 dB for the aggregates of needles. After reaching their maxima at median volume diameters around 5 to ~~10~~7 mm, ~~before doubling~~ the triple-frequency radar signatures double back such that most curves are non-unique ~~with~~ in DWR_{35-95} while DWR_{10-35} continues to increase with median particle size. This ~~“hook”~~ hook feature in the triple-frequency radar signature is characteristic of aggregates in theoretical and observational studies [e.g. *Kneifel et al.*, 2015]~~. The~~ , and the concavity of the hook feature increases with both PSD shape parameter for fractal particles (Fig. 3 a & d) and density factor (Fig. 3 b ~~)~~& e). This saturation of DWR_{35-95} for aggregates is expected to pose a challenge for dual-frequency retrievals with 35 and 95 GHz radars, such that it will be difficult to differentiate moderately-sized from very large aggregates. This effect would not be aided by the assimilation of mean Doppler velocity, because the terminal fall speed of the largest unrimed aggregates also saturates [e.g. *Mitchell and Heymsfield*, 2005]. The triple-frequency radar signature is

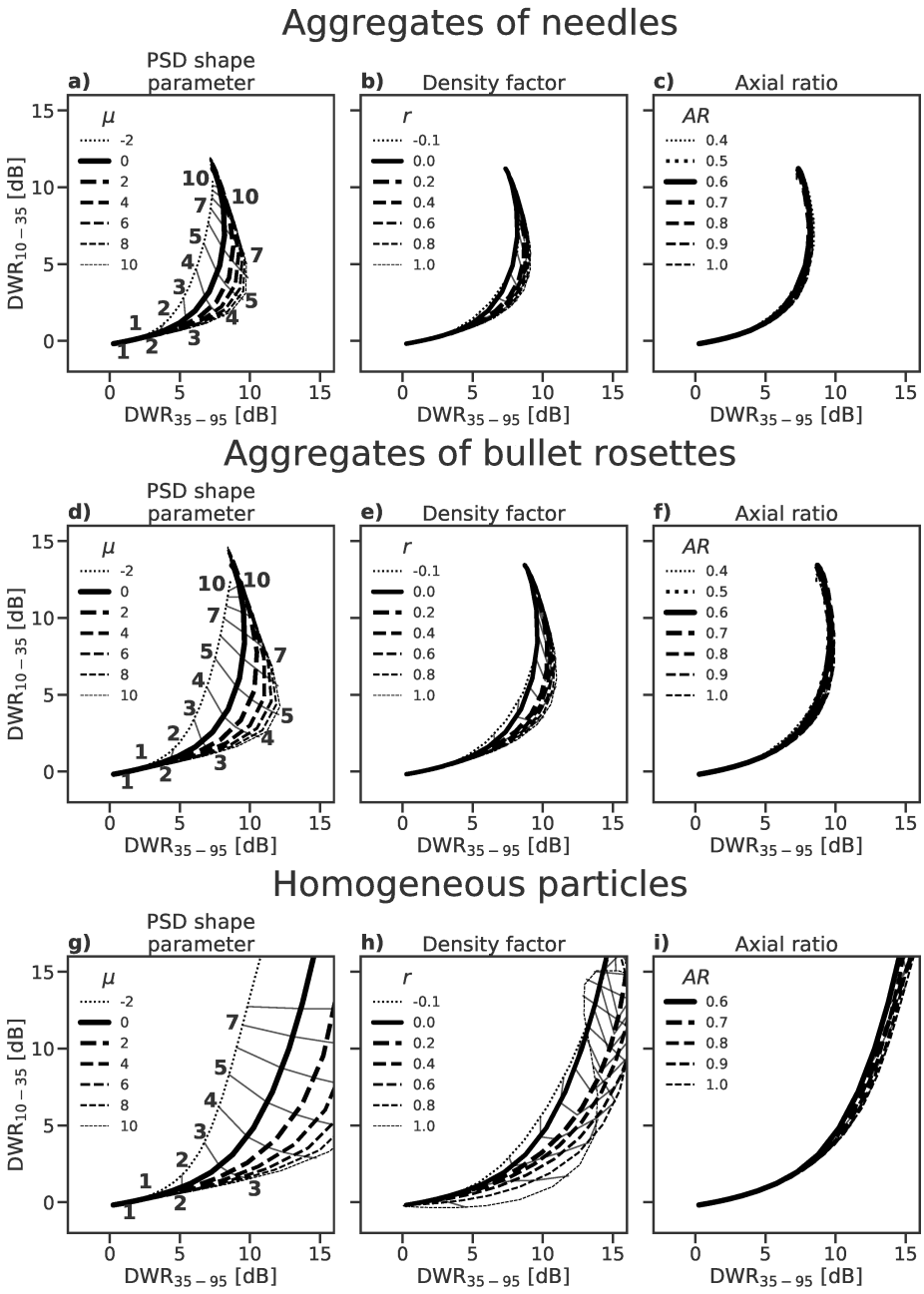

Figure 3. Simulated triple-frequency radar signatures for distributions of (a–c) fractal particles represented using SSRGA and (d–f) homogeneous ("soft") spheroids. Black lines illustrate radar signatures for a spectrum of PSDs with median volume diameters (values indicated in panels a and d) for different values of (a, d & g) PSD shape parameter, (b, e & h) density factor, and (c, f & i) axial ratio. Lateral lines denote increments of median volume diameter in millimeters.

relatively insensitive to the axial ratio of the spheroidal particles (Fig. 3 c & f). The triple-frequency signatures differ ~~due to changing values of~~ with particle density and PSD shape ~~factor~~ parameter between median volume diameters of 2 mm and 8 mm, but converge outside this range. Increasing the PSD shape parameter results in greater maximum values of DWR_{35-95}: while an exponential PSD reaches a maximum of around 9 dB at a median volume diameter around 7 mm, narrower PSDs reach DWR_{35-95} of up to 12 dB at median volume diameters around 5 mm. A smaller range of triple-frequency signatures is attributable to changes in the density factor: low-density ~~fractal particles~~ aggregates of bullet rosettes exhibit a maximum ~~DWR_{35-95}~~ DWR_{35-95} of around 9 dB at 7 mm median volume diameter, and increase to around 11 dB for denser particles with $r > 0.4$~~.~~; the maximum DWR_{35-95} of aggregates of needles increase from around 7 to 8 dB. We note that the SSRGA snowflake model is suited to low-density aggregate particles; at higher density factors the Rayleigh-Gans approximation is no longer valid due to the interaction between dipoles within the particle. An evaluation of the suitability of SSRGA to dense rimed particles is assessed in *Leinonen et* al. [2018b].

The flat signatures of homogeneous spheroids reach greater values of DWR_{35-95} than the fractal particles, even at relatively small median volume diameters of 3 to 4 mm. The triple-frequency radar signature for homogeneous spheroids resembles that shown in Fig. 1 for aggregate particles with either a power law amplitude of $\beta = 0$ or a power law exponent of $\gamma = 4$. This similarity is maintained up to density factors around $r = 0.5$, where the interaction between dipoles in the homogeneous particles becomes non-negligible. Both PSD shape ~~and density~~ parameter and density factor affect a shift of the signature to the lower-right of the diagram ~~; and~~and, unlike fractal particles, the signatures of homogeneous spheroids do not converge at large median volume diameters. ~~The density factor tends to increase the DWR~~Increasing the density factor of homogeneous spheroids increases DWR_{35-95} ~~for homogeneous spheroids~~ ; however, the hook feature only becomes evident for high density factors at large median volume diameters. Notably, at very high density factors $\mathrm{DWR}_{10-35} \approx 0$ dB are maintained for values of DWR_{35-95} up to around 10 dB: this characteristic signature of very dense graupel is not observed for very high PSD shape parameters.

Regardless of particle structure, the ~~aspect ratio~~ axial ratio (AR) of the particles has a relatively minor influence on the triple-frequency signature. We therefore maintain the assumption of $AR = 0.6$ for all particles in this study, but note that uncertainty in this value contributes to uncertainties in the retrieval in other respects. For example, *Mason et al.* [2018] found that assuming $AR = 0.8$ leads to a roughly 20% increase in retrieved ice water content when compared to $AR = 0.6$. In situ measurements show that heavily rimed and graupel particles tend to have higher ~~aspect~~ axial ratios [e.g. *Garrett et al.*, 2015; *Li et al.*, 2018], so including this effect in future retrievals may help to constrain uncertainties in estimates of dense rimed snow.

~~The range of radar signatures is overlaid with the measured triple-frequency radar data from Hyytiälä; it is clear that neither fractal particles nor homogeneous spheroids can entirely represent the~~ While no one particle morphology can represent the wide range of measured triple-frequency radar signatures ~~, but also that there exists~~ [*Dias Neto et* al., 2019], there is also significant ambiguity between the radar signatures ~~at all particle~~ of small particle of all types, especially for median volume diameters less than around 3 mm. This makes the application of triple-frequency radar retrievals especially relevant to snow, rather than cloud ice. In an attempt to encompass ~~this variability—acknowledging~~ the continuum of particle types—acknowledging that the structure and density of ice particles are interrelated—*Mason et al.* [2018] formulated a hybrid representation which transitions

from fractal particles at low density factors ($r < 0.2$) to represent unrimed and lightly rimed aggregates, to homogeneous spheroids at high densities ($r > 0.5$) representing graupel-like particles. Intermediate moderately rimed aggregates in the range $0.2 < r < 0.5$ ("hybrid particles" in Fig. 4 a) are represented by an external mixture of the backscatter cross-sections of the fractal and homogeneous models. More detailed parameterisations of this continuum may be achieved using the representation of a range of aggregates with different degrees of riming [*Leinonen and Szyrmer*, 2015; *Leinonen et* al., 2018b], or fractal structures [*Leinonen and Moisseev*, 2015; *Hogan et al.*, 2017], and should be the subject of further work.

~~For both fractal particles and homogeneous spheroids,~~ We have shown that, based on simulated radar backscatter cross-sections, the PSD shape parameter has a greater influence on the simulated triple-frequency radar signature than the well-known effect of particle density. This result holds for the aggregate snowflakes modelled as fractal particles and for graupel-like particles modelled as homogeneous spheroids. The effect of the PSD shape parameter is independent of the particle morphology, but results from changing the relative weighting of different parts of the particle size spectrum. ~~To illustrate this effect, the radar backscatter cross-section ratio spectra~~ This can be shown using the dual wavelength ratio on a per-particle basis, which we call the dual backscatter ratio following *Kneifel et* al. [2016],

$$\mathrm{DBR}_{1,2} = \left(\frac{f_2}{f_1}\right)^4 \frac{\sigma_{f_1}(D)}{\sigma_{f_2}(D)}, \tag{9}$$

in which the spectral features correspond to the onset of non-Rayleigh scattering at the higher frequency [*Kneifel et* al., 2016]. $\mathrm{DBR}_{10,35}$ and $\mathrm{DBR}_{35,95}$ for fractal particles (aggregates of bullet rosettes) and homogeneous spheroids with $r = 0$ and $AR = 0.6$ are compared in Fig. 4~~cf. the triple-frequency Doppler backscatter spectra studied by *Kneifel et* al., 2016. The ratios between radar backscatter cross-sections at 10–35 GHz and 35–95 GHz (Fig. 4~~ a ~~) are shown~~ alongside the volume-weighted particle size distributions for selected PSDs (Fig. 4 b): the exponential PSD [*Marshall and Palmer*, 1948], and PSDs measured during the ~~pre-frontal and frontal~~ rimed and unrimed snow regimes of the 21 February 2014 case at Hyytiälä, Finland, which is considered in more detail in Section ~~??. The frontal~~ 4. The unrimed snow regime fits a broader Gamma PSD (e.g. $\mu = -1$), and the ~~prefrontal~~ rimed snow a narrower PSD (e.g. $\mu = 5$). As radar measurements relate to PSD-weighted integrals of the radar backscatter spectra by (1), the triple-frequency signature is strongly influenced by the median volume diameter and shape parameters of the PSD, with the PSD shape parameter modulating the relative influence of spectral features close to the median volume diameter. As the median volume diameter approaches the onset of non-Rayleigh scattering at ~~95-GHz~~ 95 GHz (around 3 mm), DWR_{35-95} increases, creating the initial horizontal part of the triple-frequency radar signatures of both fractal particles and homogeneous spheroids; correspondingly, at the onset of non-Rayleigh scattering at the ~~35-GHz~~ 35 GHz (around 8 mm) there is a shift to larger values of DWR_{10-35}, and a vertical uptick in the triple-frequency diagram. For fractal particles (dashed lines in Fig. 4 a) there is a clear distinction between the parts of the spectrum dominated by non-Rayleigh scattering at ~~95- and 35-GHz~~95 and 35 GHz: the decrease in the ~~35–95-GHz~~ 35–95 GHz backscatter cross-section ratio at median diameters greater than around 6–8 mm results in the "bending-back" part of the hook feature in the triple-frequency signature, which occurs at smaller median diameters for narrower PSD ~~shapes~~ shape parameters (Fig. 3 a).

For homogeneous spheroids (solid lines in Fig. 4 a) the many narrow features of the backscatter cross-section ratio spectra are smoothed out when integrated across the PSD, resulting in a flatter triple-frequency radar signature. This illustrates how

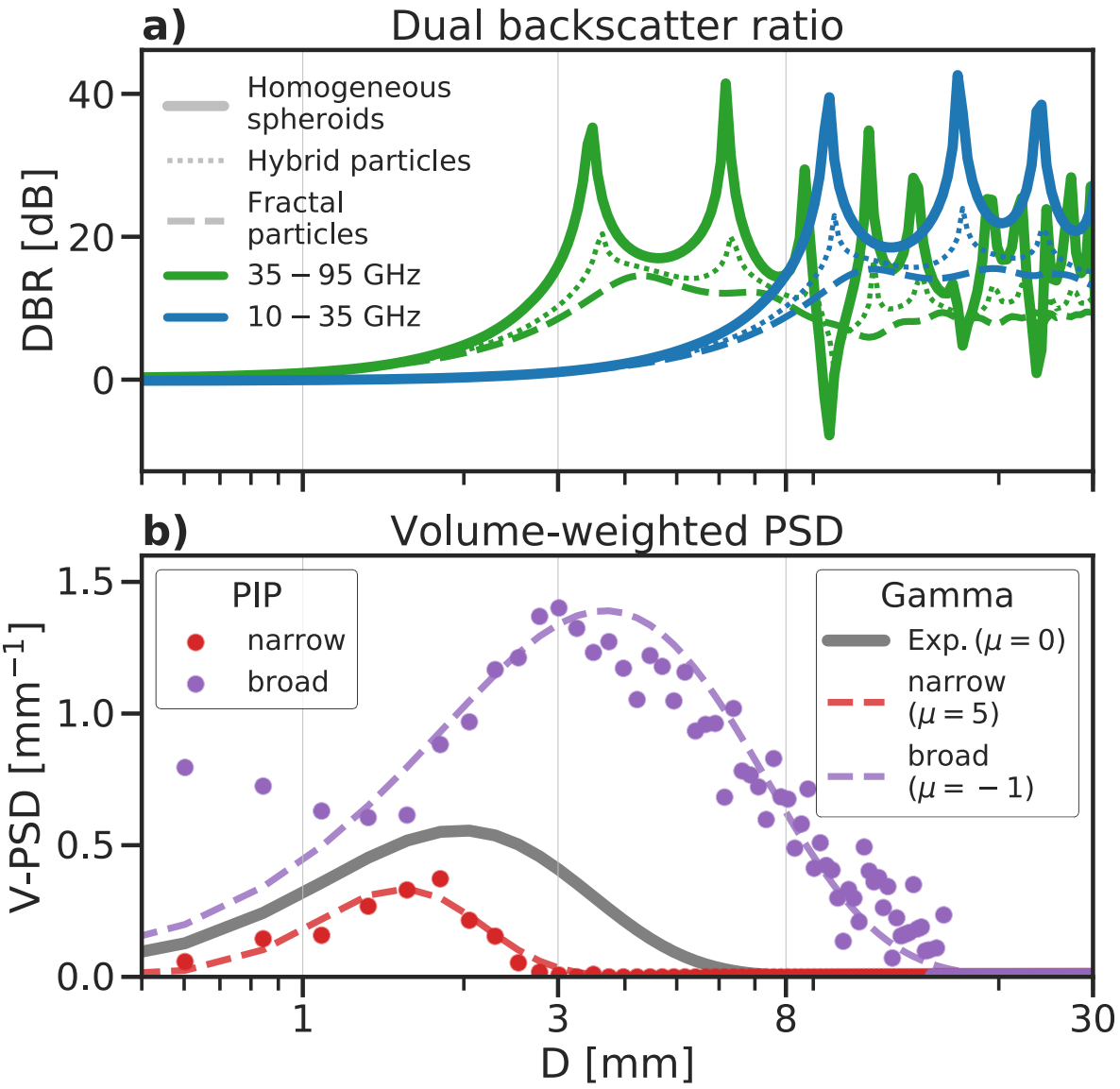

Figure 4. (a) Normalized dual backscatter ~~cross-section~~ ratios (DBR) at ~~10–35-GHz~~ 10–35 GHz and ~~35–95-GHz~~ 35–95 GHz bands for fractal particles (aggregates of bullet rosettes) and homogeneous spheroids, on the same size spectrum as (b) the volume-weighted PSD (V-PSD) measured in situ during the ~~prefrontal~~ 21 February case study (Section 4) and ~~frontal regimes and~~ Gamma PSDs fit to the same regimes, and an exponential PSD ($\mu = 0$)~~PSD~~. The backscatter cross-section ratios of the "hybrid" particles in (a) illustrate the transition between ~~fractal (SSRGA)~~ aggregates of bullet rosettes and homogeneous ~~or "soft"~~ spheroid approximations for intermediate density factors between $0.2 < r < 0.5$, as described in *Mason et al.* [2018].

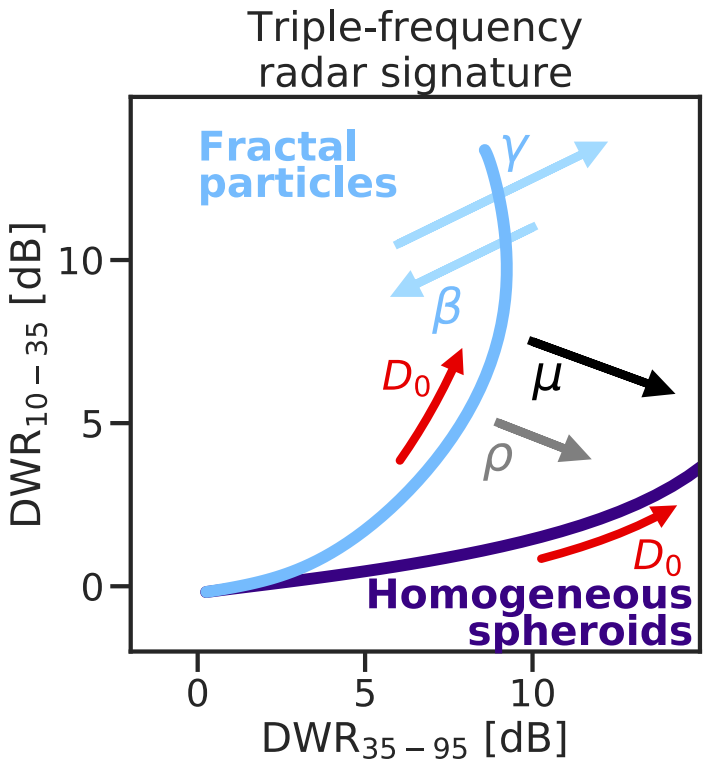

Figure 5. A schematic for the parameters affecting the triple-frequency radar signature of a spectrum of ice particles. In addition to the median volume diameter and density, the effects of ~~particle~~ the internal structure of aggregate particles and the PSD shape parameter are illustrated [cf. *Kneifel et al.*, 2015].

a narrower PSD will increase the weight given to particles closest to the median volume diameter, exaggerating the effects of nearby features of the radar backscatter spectra and deepening the hook feature characteristic of fractal particles as PSD shape parameter increases. Conversely, broader PSDs have the effect of smoothing over the spectral features, producing an earlier onset of high values of DWR_{10-35} and a shallower hook feature for fractal particles.

We may therefore add to the diagram for the triple-frequency radar signature proposed in *Kneifel et al.* [2015] to include the ~~effect of PSD shape as well as~~ effects of the PSD shape parameter and the internal structure of aggregate snowflakes, in addition to the effects of particle density (Fig. 5). ~~This reflects a significant insight~~ These reflect important insights into the interpretation of triple-frequency radar signatures~~, as~~: it is possible that the observed range of measurements in *Kneifel et al.* [2015] are attributable to the combined effects of increased particle density due to riming~~and a narrow PSD~~, of a narrower or broader PSD, and of variations in the internal structure of aggregate snowflakes. It is not apparent to ~~which~~ what degree these parameters are independent of one another~~, although~~: *Tiira et al.* [2016] found only a weak relation between the bulk density and PSD shape ~~factor~~ parameter estimated from PIP measurements at Hyytiälä. ~~This poses a~~ Each of these effects represent

an additional challenge when seeking to retrieve the morphology of particles from the triple-frequency radar measurements, a problem we will explore further in the next ~~section~~sections.

4 ~~Case~~ Retrievals of density factor and the PSD shape parameter: 21 February 2014 case study

~~In this section we revisit one of the triple-frequency radar case studies from Hyytiälä, Finland, explored by *Kneifel et* al. [2015].~~ ~~The~~ Between 22:53 and 23:17 UTC on 21 February 2014 ~~case has been widely studied with remote-sensed~~ light snowfall dominated by compact graupel gave way to moderate snow characterised by larger unrimed aggregates [see Section 3.5.1 of *Kneifel et* al., 2015, for a detailed discussion of the meteorological context and in situ observations ~~because it includes the transition from heavily rimed to unrimed snow during the passage of a front. The 25-minute period of triple-frequency~~ of this case]. *Mason et* al. [2018] exploited Doppler velocity during a longer time series of this event to constrain CAPTIVATE retrievals of the density factor, using single- and dual-frequency Doppler radar measurements~~(Figure 6) are separated into prefrontal~~. We divide the 25 minute case into rimed (22:53 to 23:03 UTC) and ~~frontal~~ unrimed regimes (23:03 to 23:18~~UTC) regimes.~~ UTC) based on a combination of remotely-sensed (Fig. 6) and in situ data. *Kneifel et al.* [2015] showed that the onset of unrimed ~~frontal~~ snow corresponded to the emergence of the distinct hook feature in the triple-frequency signature~~, simultaneous with a reduction in particle fallspeeds observed both in situ and by~~. This corresponds to the large values of both DWR_{35-94} and DWR_{10-35} (Fig. 6b & c) near the surface during the unrimed snow regime, where mean Doppler velocity ~~. *Mason et* al. [2018] exploited the Doppler velocity to constrain an estimate of the density factor in the context of single-~~ is between 1 and ~~dual-frequency radar retrievals of a longer time series of the same case. Here we use the~~ $1.5\,\mathrm{m\,s^{-1}}$ (Fig. 6d). In contrast during the rimed regime very high values of $\mathrm{DWR}_{35-95} > 10$ dB around 3 km above ground level correspond to a rapid increase in mean Doppler velocity up to around $2\,\mathrm{m\,s^{-1}}$. We use this case study to consider the importance of the ~~PSD~~ density factor, particle structure and PSD shape parameter to the triple-frequency ~~signature~~ signatures of the two regimes (Section ~~??~~4.1), and ~~then attempt a retrieval of particle density and PSD shape~~ evaluate the capability to resolve changes in PSD shape parameter, as well as the density and internal structure, from triple-frequency ~~Doppler radar~~ radar reflectivity measurements (Section 4.2).

4.1 Triple-frequency radar signatures

In Section 3 we ~~showed that the PSD shape has a greater influence~~ explored the influences of various factors on the triple-frequency radar signature~~than the density factor, but we~~ , but did not consider the expected ~~range of observed~~ ranges of values for each of these parameters, nor how they may co-vary. Here we use in situ and ~~remote-sensed measurements from the case study~~ remotely-sensed measurements to explore the ~~range of~~ size distributions and particle morphologies that best ~~explain~~ represent the observed triple-frequency radar signatures.

~~We make a coarse distinction between the prefrontal regime before 23:03 UTC, and the frontal regime thereafter. Triple-frequency radar measurements (Fig. 6) show an increase in 10 and 35-GHz radar reflectivities with the onset of frontal snowfall, while~~

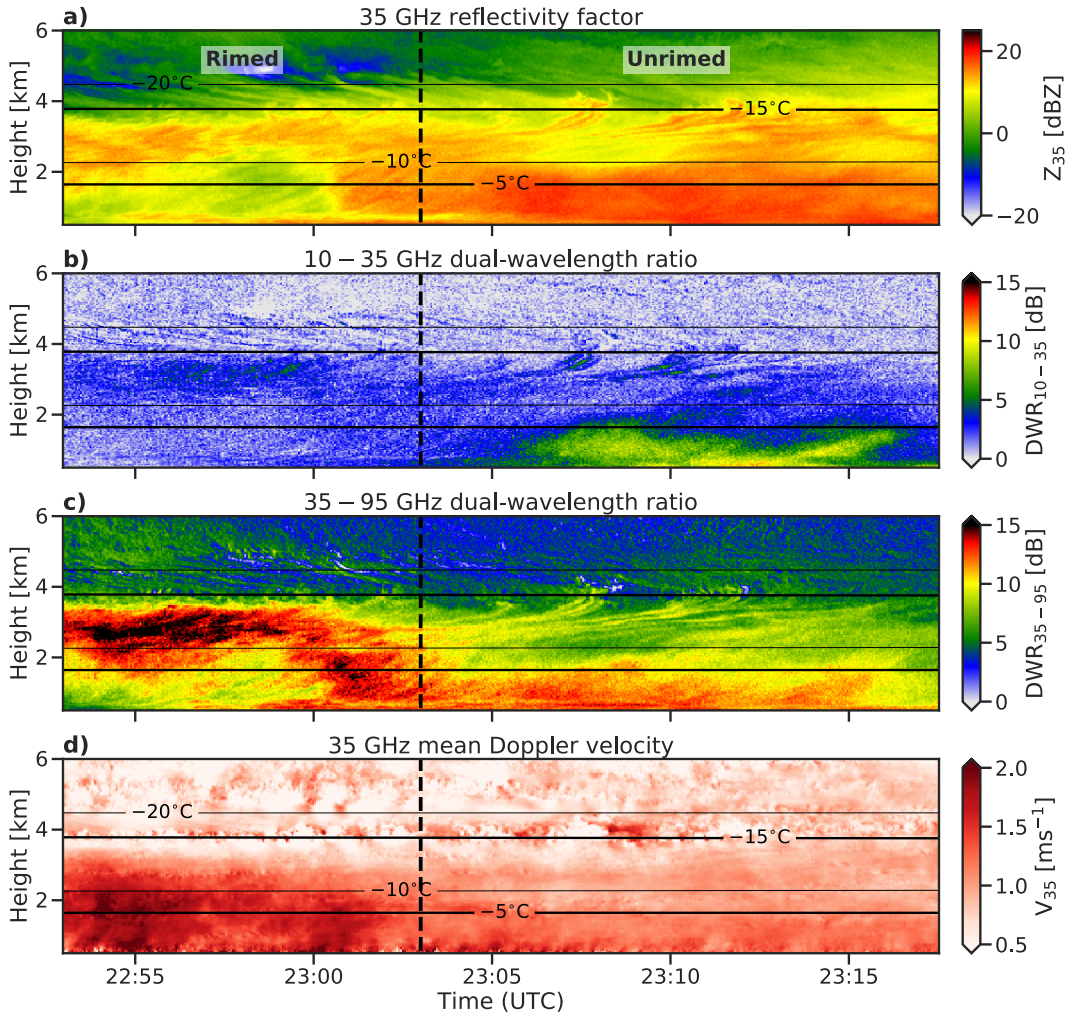

Figure 6. Triple-frequency Doppler radar measurements from the February 21 2014 case study at Hyytälä, Finland. (a) ~~35-GHz~~ 35 GHz radar reflectivity, (b) ~~10–35-GHz~~ 10–35 GHz dual wavelength ratio, (c) ~~35–95-GHz~~ 35–95 GHz dual wavelength ratio, and (d) ~~35-GHz~~ 35 GHz mean Doppler velocity. ~~Dashed~~ Vertical dashed lines mark the transition between the ~~prefrontal~~ heavily rimed and ~~frontal~~ large aggregate snowfall regimes; solid lines are contours of temperature from ECMWF analysis.

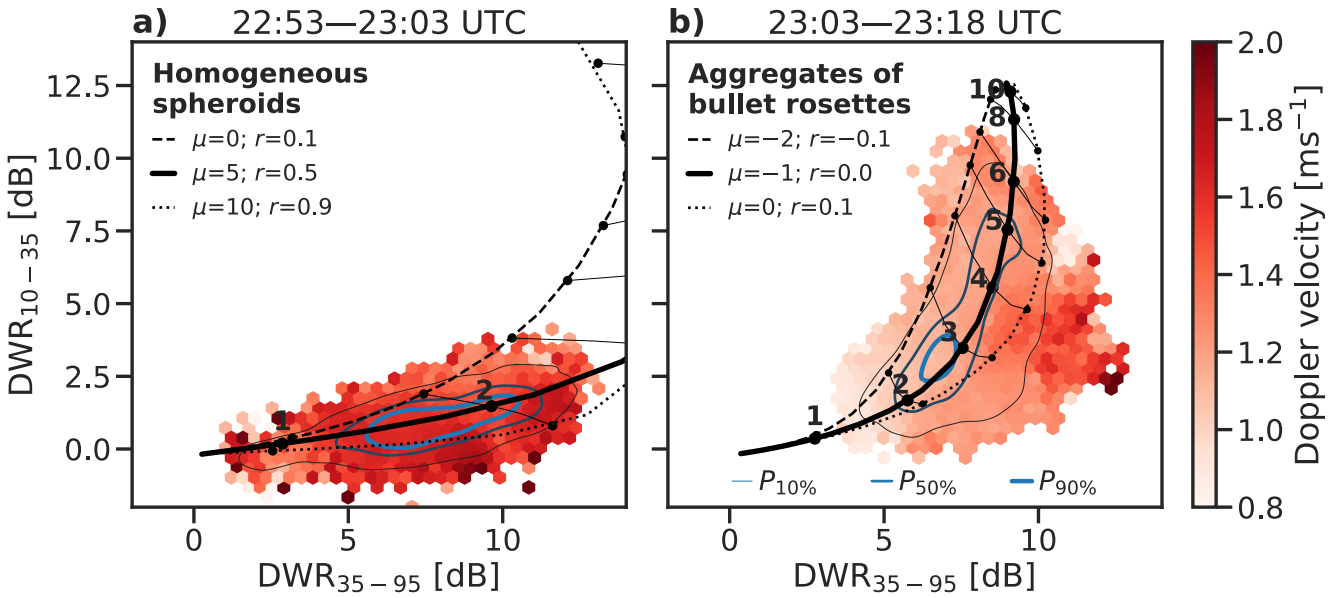

Figure 7. Triple-frequency radar measurements below 2 km above ground level in the (a) ~~prefrontal~~ rimed and (b) ~~frontal~~ unrimed snow regimes of the 21 February 2014 case at Hyytiälä, Finland. Triple-frequency radar measurements are coloured by the corresponding mean Doppler velocity, and frequency of occurrence is indicated with ~~black~~ blue contours at the 10th, 50th and 90th percentiles. Overlaid are triple-frequency radar signatures for (a) homogeneous spheroids and (b) fractal particles (aggregates of bullet rosettes; Table 1) with a range of values of PSD shape parameter and density factor that encompass the most frequent triple-frequency radar measurements. Increments of median volume diameter are labelled in millimeters.

~~the mean Doppler velocity nearest the surface decreases from around 2 m s^{-1} before the front arrives, to around 1 to 1.5 m s^{-1} during the frontal regime.~~

As a check on the representation of particle properties and radar scattering assumptions~~within CAPTIVATE~~, we evaluate the ~~capability to reproduce~~ how faithfully our model particles can reproduce the triple-frequency radar signatures ~~that resemble the triple-frequency radar measurements of~~ measured during the rimed and unrimed snow ~~during the prefrontal and frontal snow regimes. Previous analyses of in situ measurements and remote-sensed retrievals of the density factor can be used~~ regimes. We vary the particle internal structure, density and PSD shape parameters based on in situ and remotely-sensed measurements to confirm that the forward model ~~captures the particle properties as well as the~~ is capable of resolving the triple-frequency radar ~~signatures.~~

measurements. The triple-frequency radar measurements below 2 km in the ~~prefrontal~~ rimed snow regime are coloured by the average mean Doppler velocity, and contours ~~at~~ indicate the 10 th, 50 th and 90 th percentiles ~~indicate the frequency of~~

~~the triple-frequency radar measurements~~ of frequency of occurrence (Fig. 7a). The rimed ~~prefrontal~~ snow is characterised by a flat triple-frequency signature ~~in which~~ with DWR_{35-95} ~~is~~ between 5 and 11 dB ~~, with~~ and DWR_{10-35} less than 2 dB, and mean Doppler velocities between 1.5 and 2 $\mathrm{m\,s^{-1}}$~~, consistent with dense rimed particles~~. The radar measurements are overlaid with triple-frequency radar signatures for homogeneous spheroids with a range of ~~median volume diameters, PSD shapes~~ PSD shape parameters and density factors~~. The bulk of the prefrontal snow corresponds to the~~ : the rimed snow exhibits triple-frequency radar signatures~~of~~ , consistent with homogeneous spheroids with a density factor of $r = 0.5$ ~~, consistent with compact graupel-like particles retrieved by *Mason et* al. [2018];~~ [as retrieved from mean Doppler velocity in *Mason et* al., 2018] and a PSD shape parameter of $\mu = 5$ ~~, which was measured~~ as measured by PIP at the surface ~~during this period~~ (Fig. 4~~). Most of the~~ b). 90% of the triple-frequency radar measurements correspond to median volume diameters between ~~2~~ 1.5 and 3 mm, consistent with PIP measurements ~~during this period~~ [*Kneifel et al.*, 2015, and shown later in Fig. 10e.].

The ~~frontal~~ unrimed snow regime (Fig. 7b) exhibits the hook feature characteristic of unrimed aggregates, with most measurements of DWR_{35-95} between 5 and 10 dB and DWR_{10-35} up to around ~~8~~10 dB. The most frequent triple-frequency radar measurements are a good fit to aggregates of bullet rosettes with a PSD shape parameter with $\mu = -1$ (measured in situ), and a density factor of $r = 0$. In contrast to the rimed ~~prefrontal~~ snow, this regime ~~exhibits~~ is dominated by lower mean Doppler velocities between 1 and 1.5 $\mathrm{m\,s^{-1}}$, ~~but includes some~~ consistent with the low terminal velocities of even large aggregate snowflakes; less than 10% of the triple-frequency radar measurements ~~at higher~~ include values of DWR_{35-95} greater than 10 dB and mean Doppler velocities greater than 1.5 $\mathrm{m\,s^{-1}}$, suggesting ~~that some rimed particles persist~~ a small amount of rimed particles persisting after 23:03 UTC. The ~~most frequent~~ triple-frequency radar measurements ~~are a good fit to fractal particles with a PSD shape with $\mu = -1$, which was measured in situ during the frontal regime; and a density factor of $r = 0$, corresponding to unrimed aggregate snowflakes. The triple-frequency radar measurements~~ correspond to fractal particles with median volume diameters ~~as small as~~ from 1.5 mm ~~and as large as~~ to 8 mm, but ~~the majority~~ 90% of the data ~~suggest~~ lie within the range expected for fractal particles with median diameters between ~~3 and 5~~2 and 7 mm~~, which~~ . This is consistent with in situ PIP measurements at the surface (Fig. 10e).

Comparing our particle models ~~parameterised by density factor and PSD shape~~ against measured triple-frequency radar measurements for a case study, it is evident that the rimed ~~prefrontal~~ snow is well-represented by a narrow PSD comprising of dense graupel-like particles with a median volume diameter around 1 to 2 mm. ~~In contrast, the frontal~~ The unrimed snow corresponds to a broad distribution of large ~~unrimed~~ aggregates with median volume diameters between 3 mm and 8 mm. The fit to triple-frequency radar signatures requires a representation of the PSD shape parameter, particle density and microphysical structure, illustrating that it is necessary to include variability in the PSD shape ~~is key to resolving~~ parameter to resolve the triple-frequency radar signatures of snow.

4.2 Triple-frequency radar ~~retrieval~~retrievals

In this section we perform ~~an optimal estimation retrieval constrained by~~ CAPTIVATE retrievals of the 21 February case using triple-frequency and Doppler radar measurements. *Mason et al.* [2018] used ~~a~~ dual-frequency radar ~~reflectivity~~ reflectivities to constrain two parameters of the PSD, while the density ~~factor was~~ factor—and hence the particle structure—were constrained

by mean Doppler velocity at one ~~radar~~ frequency. Following the studies of ~~*Leinonen et* al. [2018]~~ *Leinonen et* al. [2018a] and *Tridon et al.* [2019], we are interested in whether the triple-frequency radar ~~measurments~~ measurements can be used to constrain a retrieval of particle density, or if—given the evidence presented above—it will ~~be essential to include information about~~ instead be necessary to vary the PSD shape parameter in order to satisfy the triple-frequency constraint. ~~If the major parameters controlling the triple-frequency signature were represented within a radar forward-model, an optimal estimation retrieval could be made to estimate those parameters, if adequately constrained by the measurements. With a secondary means of estimating the particle density from the mean Doppler velocity, we can compare estimates of particle density based on their ability to forward-model the measured mean Doppler velocity.~~

~~We~~

4.2.1 Retrievals assuming constant PSD shape parameter

We first perform retrievals assimilating a variety of radar measurements in order to compare their respective contributions. The default retrieval combines radar reflectivity at 10, 35 and ~~95 GHz~~ 95 GHz and mean Doppler velocity at ~~35 GHz~~ 35 GHz ($Z_{10,35,95}\,V_{35}$), which represents the full available measurement vector. As explained in Section 2.2, 95 GHz Doppler velocity measurements are affect by a mispointing; we therefore assimilate mean Doppler velocity from the 35 GHz radar only, and do not consider the contribution of multiple Doppler velocity measurements to this retrieval. To test the capability to retrieve ~~the~~ particle density from triple-frequency radar reflectivity factors, we also make a retrieval which does not assimilate Doppler velocity (i.e. $Z_{10,35,95}$); and to test the contribution of the third radar frequency, we test dual-frequency retrievals (i.e. $Z_{10,35}\,V_{35}$ and $Z_{35,95}\,V_{35}$). Reducing the number of measurements assimilated may lead to a more challenging inverse retrieval problem, wherein either the measurement vector provides insufficient constraint on an estimate of the state vector, or the state space does not include a solution that satisfies all of the measurements.

The quality of the retrieval ~~may be~~ is illustrated by comparing the measurements against those forward-modelled from the retrieved state. We take representative profiles from each snow regime: a ~~prefrontal~~ profile characterised by rimed snow (23:00 UTC; Fig. 8), and ~~a frontal profile~~ one dominated by large unrimed aggregates (23:10 UTC; Fig. 9). The profiles of retrieved variables are shown in the supplementary material.

Comparing retrievals of the ~~prefrontal~~ rimed profile with an exponential PSD (Fig. 8 a–d), ~~it is evident that~~ the triple-frequency retrievals $Z_{10,35,95}\,V_{35}$ and $Z_{10,35,95}$ ~~are not able to~~ do not satisfy all three profiles of radar reflectivity simultaneously, with errors of 1 to 2 dB~~, while the~~ . The dual-frequency radar retrievals $Z_{35,95}\,V_{35}$ and $Z_{10,35}\,V_{35}$ ~~are able to~~ satisfy the assimilated radar frequencies, but exhibit large errors in the remaining frequency (e.g. up to 4 dB in forward-modelled DWR_{10-35} for $Z_{35,95}\,V_{35}$). ~~$Z_{10,35}\,V_{35}$ and $Z_{35,95}\,V_{35}$ are both well-constrained, and the~~ The profiles forward-modelled by $Z_{10,35,95}\,V_{35}$ resemble a compromise between the ~~95 and 10 GHz~~ dual-frequency retrievals, but satisfying neither: this is indicative of an over-constrained retrieval, in which the state space does not permit a solution that satisfies all of the observational constraints. The retrievals assimilating Doppler velocity have adequate constraints on the density factor to represent the observed increase in mean Doppler velocity below around 3 km above ground level. $Z_{10,35,95}$ is similar to $Z_{10,35,95}\,V_{35}$ in terms of radar reflec-

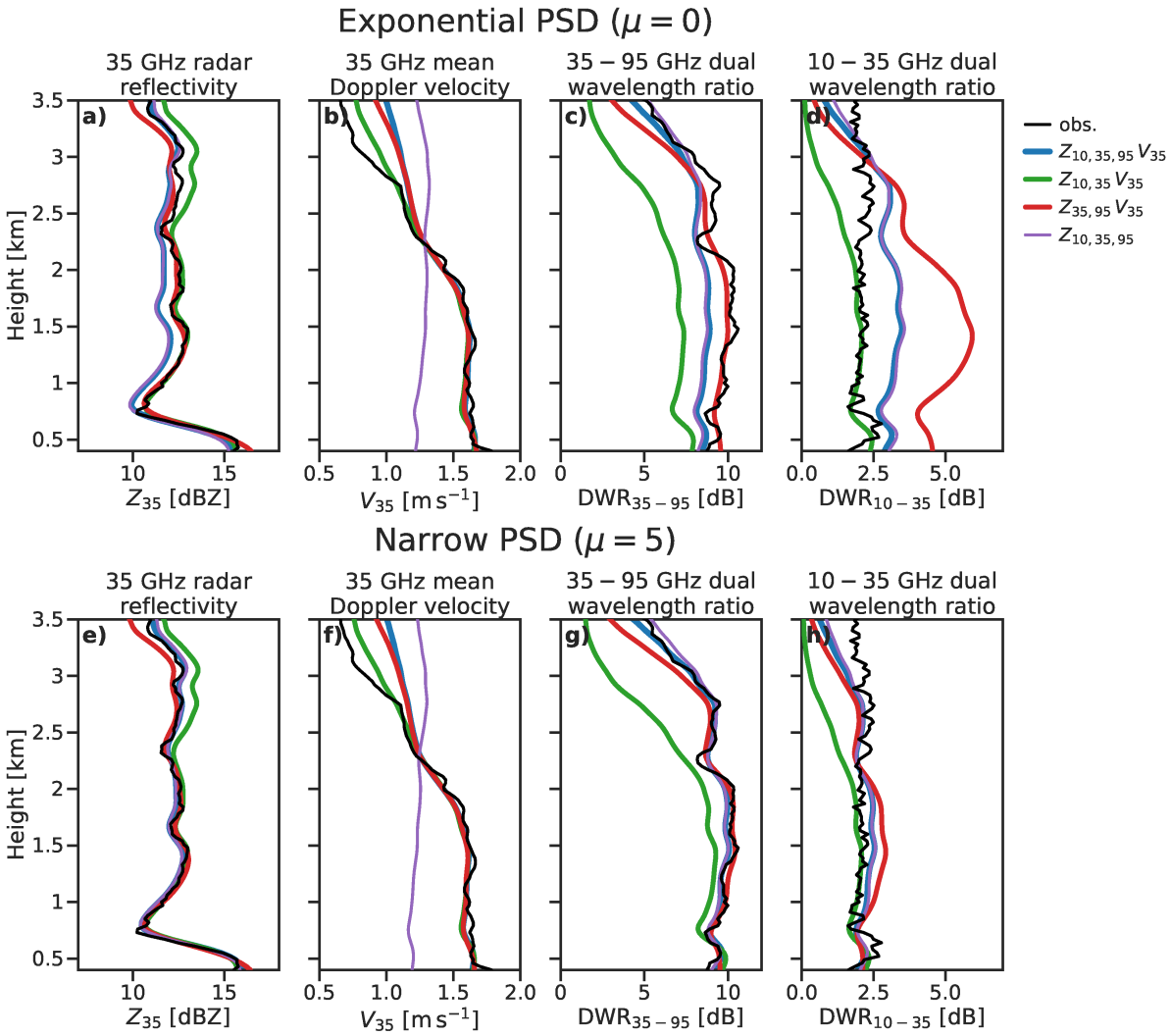

Figure 8. Profiles of observed and forward-modelled radar variables for retrievals of a selected profile during the ~~prefrontal~~ rimed snow regime. Retrievals assuming (a–d) an exponential PSD are compared against those with (e–h) a narrow PSD with $\mu = 5$.

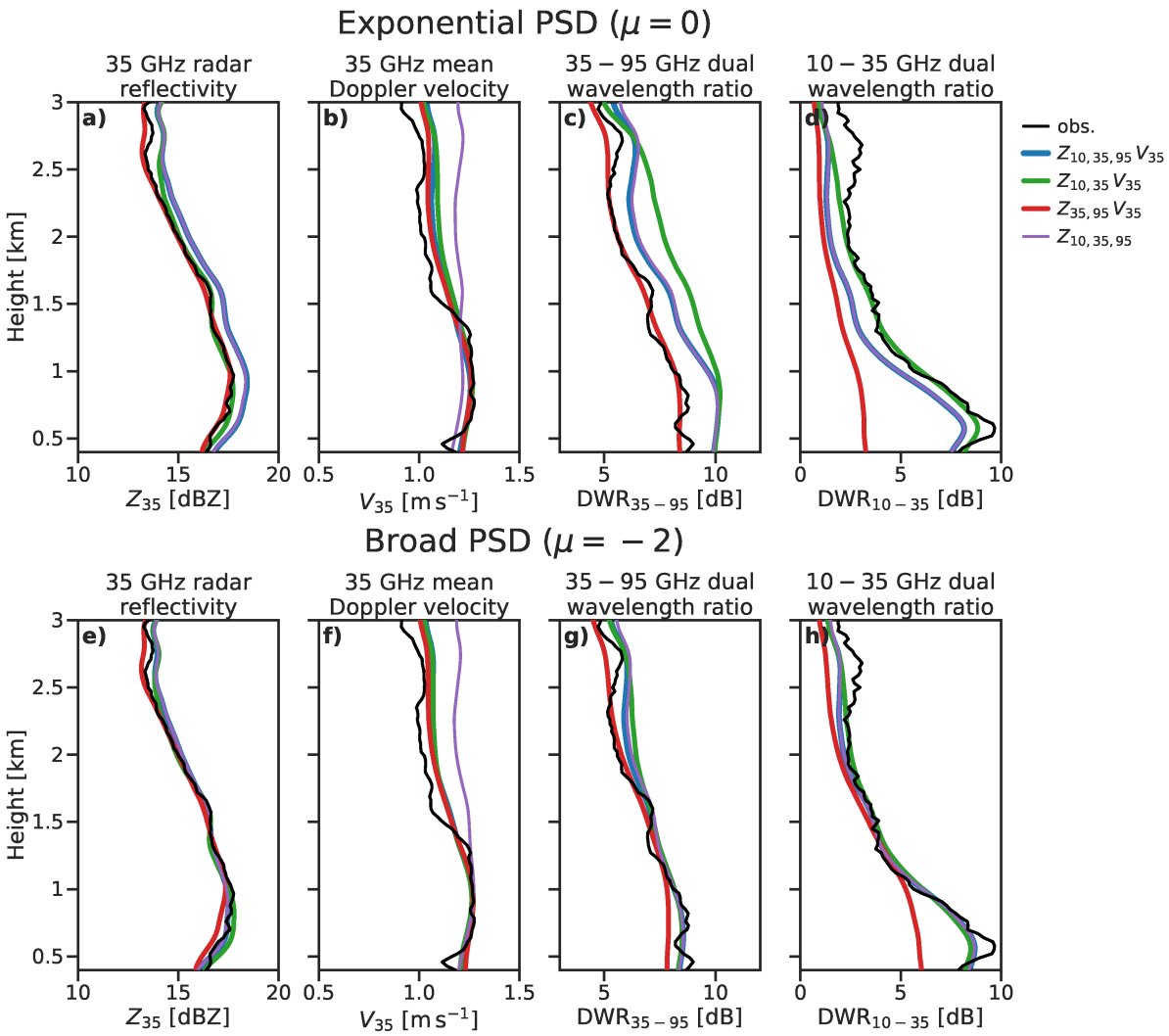

Figure 9. Profiles of observed and forward-modelled radar variables for retrievals of a selected profile during the ~~frontal~~ unrimed snow regime. Retrievals assuming (a–b) an exponential PSD are compared against those with (e–h) a broad PSD with $\mu = -2$.

tivity, but the observed ~~increase in~~ profile of mean Doppler velocity, including a rapid increase to around 1.6 m s^{-1} below 2 km above ground level, is not resolved at all without assimilating ~~the~~ mean Doppler velocity.

As shown in Section ~~??~~4.1, the triple-frequency radar measurements in the ~~prefrontal~~ rimed regime are best ~~represented with narrow PSDs with~~ explained by a narrow PSD ($\mu > 5$~~, consistent with in situ measurementsat the surface~~) as indicated by PIP measurements. We therefore repeat the CAPTIVATE retrievals with constant $\mu = 5$ rather than $\mu = 0$ (Fig. 8 e–h). ~~The~~ In this retrieval the forward-modelled profiles of radar reflectivity are considerably better constrained by the measurements~~in this retrieval~~: $Z_{10,35,95}\,V_{35}$ especially is very close to all the observations. The exception is that the retrieval does not match the ~~10-GHz~~ 10 GHz reflectivity factor above around 3 km; it is likely that the PSD shape ~~changes through~~ parameter changes at this level, where the onset of ~~the riming process~~ riming is evident from increased mean Doppler velocities, and where layers of supercooled liquid have been identified in the Doppler spectra [*Kalesse et al.*, 2016]. The ~~profiles of radar reflectivity~~ forward-modelled radar reflectivity factors of the dual-frequency retrievals are also better-constrained when a narrower PSD is assumed~~; however, it~~ , indicating that single- and dual-frequency radar retrievals are also affected by the assumption of exponential PSDs. It is not evident that ~~the~~ triple-frequency radar measurements provide any significant constraint on the density factor ~~of~~ for $Z_{10,35,95}$~~:~~, as the forward-modelled mean Doppler velocity of that retrieval is unchanged.

Retrievals of the profile of unrimed ~~frontal~~ snow (Fig. 9) show similar results: when an exponential PSD is used, $Z_{10,35,95}\,V_{35}$ exhibits errors of up to 2 dB in the profiles of radar reflectivity. The retrieval is over-constrained~~with respect to triple-frequency radar measurements~~, as the state space does not allow for the triple-frequency radar signature of the large aggregates to be represented. A significant difference between the ~~frontal and the prefrontal~~ profiles is that ~~all retrievals~~ in the unrimed regime retrievals that do not assimilate Doppler velocity are able to represent the observed profile of mean Doppler velocity~~below about 1.5 km, showing that the prior density factor of~~ : this is because the a priori density factor ($r = 0$~~makes an accurate~~) makes a reasonable estimate of the terminal fallspeed of unrimed aggregate particles, provided that their size is well-constrained by dual-frequency radar ~~measurements—even when mean Doppler velocity measurementsare not assimilated. Above~~ measurements. However, above 1.5 km ~~, $Z_{10,35,95}$~~ the non-Doppler retrieval over-estimates the mean Doppler velocity by around 0.2 m s^{-1}~~. As for~~ , while retrievals that assimilate Doppler velocity estimate negative values of riming factor (Fig. A2d), attributing weaker Doppler velocities above this level to lower-density aggregate snowflakes. As was shown for the rimed regime, all the ~~prefrontal profile, all of the~~ retrievals are better able to represent the triple-frequency radar measurements when a non-exponential PSD is used~~;~~ : here, assuming a broader PSD ~~with~~ ($\mu = -2$) results in consistently better-constrained retrievals at all three radar frequencies. One exception is that the $Z_{35,95}\,V_{35}$ retrieval is profoundly unable to resolve the very high values of DWR_{10-35} below about 1 km above ground level. Profiles of retrieved variables (Fig. A2) show that this is due to a failure to resolve the very large aggregates in this part of the profile, to which which the DWR_{10-35} is most sensitive. This is a result of the hook feature of the triple-frequency radar signature of aggregates, in which DWR_{35-95} is quickly saturated around 7 to 10 dB. In this situation the third radar frequency provides an important constraint on the size of large aggregate snowflakes.

These results indicate that, at least as the retrieval is configured here, triple-frequency radar measurements are insufficient to constrain a retrieval of the density factor. This is consistent with the results of ~~*Leinonen et* al. [2018]~~*Leinonen et* al. [2018a], wherein the retrieved prefactor of the particle mass-size relation was relatively insensitive to the triple-frequency radar mea-

surements. ~~Instead, the~~ However, assimilating mean Doppler velocity at one radar frequency provides an effective constraint on the density ~~of rimed snow, as~~ and structure of snowflakes, as was shown in *Mason et al.* [2018]. ~~Furthermore~~

Secondly, we have shown that ~~the retrieval may be ill-posed if all ice is assumed to have~~ even when the density factor and particle structure are retrieved, the retrieval can be over-constrained due to the assumption of an exponential PSD~~: that~~. That is, because the PSD shape ~~has more~~ parameter has a significant influence on the triple-frequency radar signature ~~than the density of ice particles~~(Section 3), it may not be possible to retrieve a state vector that satisfies all three radar frequencies unless the PSD shape parameter can also be estimated, such as from in situ measurements.

4.2.2 Retrieval of the PSD shape parameter

We have shown that over-constrained retrievals in both the ~~prefrontal and frontal~~ rimed and unrimed profiles were improved by ~~using in situ measurements to update the PSD shape, which~~ matching the PSD shape parameter to concurrent PIP measurements at the surface. In CAPTIVATE the PSD shape parameter is assumed constant ~~within CAPTIVATE retrievals~~ in each retrieval, but can be configured at runtime. ~~Further~~At least for this case study, we have also confirmed that our models for aggregate snowflakes and ~~graupel-like particles allow for~~ homogeneous spheroids allow a good representation of ~~their~~ triple-frequency radar signatures ~~when both~~ in conjunction with density and PSD shape ~~are modified.Within an optimal estimation retrieval it therefore~~ parameter (Fig. 7). Since the mean Doppler velocity is used to estimate the density factor and particle structure, it should be possible to minimise errors in the forward-modelled ~~profiles of~~ triple-frequency radar measurements~~to constrain the PSD shape in addition to the median volume diameter and normalized number concentration, which are well-constrained in dual-frequency retrievals. While CAPTIVATE is not currently configured to easily retrieve~~ , in order to estimate the PSD shape ~~as a state variable, we can~~ parameter. We carry out a pseudo-retrieval by running multiple $Z_{10,35,95}\,V_{35}$ retrievals in which ~~PSD shape is assumed to take~~ the PSD shape parameter takes integer values from $\mu = -2$ to $\mu = 10$. The ~~pseudo-retrieval is made by selecting the value of PSD shape that~~ retrieved value is that which minimises the error in forward-modelled DWR_{35-95} and DWR_{10-35} between 400 and 600 m above ground level (Fig. 10a & b)~~; the state vector is linearly interpolating between the retrieved state vectors at the retrieved value~~ . The forward-modelled DWRs for a range of PSD shape ~~, giving an estimate of the other retrieved quantities when the PSD shape is retrieved (Fig. 10~~parameters span up to 4 ~~d–g).~~ dB, with the range depending on the median volume diameter. To reduce noise in the pseudo-retrieval the minimisation is carried out at a smoothed temporal resolution of 15 s. The estimated PSD shape parameter (Fig. 10 c), and the corresponding retrieved quantities (Fig. 10 d–g), are compared to PIP measurements at the surface.

The retrieved timeseries of ~~PSD (Fig. 10c)~~ the PSD shape parameter is consistent with that measured ~~at the surface, with PSD shapes from~~ by PIP, with the rimed regime associated with narrow PSDs ($3 < \mu < 10$~~reflecting narrow size distributions of snowfall in the prefrontal regime , and~~) before transitioning to broader PSDs ~~with~~ ($-2 < \mu < 0$~~after around 23:05 UTC~~) in the unrimed regime. Prior to around 23:00 UTC the retrieved PSD ~~noisy, with high uncertainties reflecting~~ shape parameter is especially noisy: high uncertainties reflect the increasingly weak distinctions between ~~PSD shapes in the timeseries of~~ forward-modelled ~~DWR~~ DWRs assuming different PSD shape parameters (Fig. 10 a & b)~~; this~~ . This is because, as observed in Figs. 3 & 4, the triple-frequency radar signatures converge at median volume diameters less than around 2 mm, ~~the sizes at~~

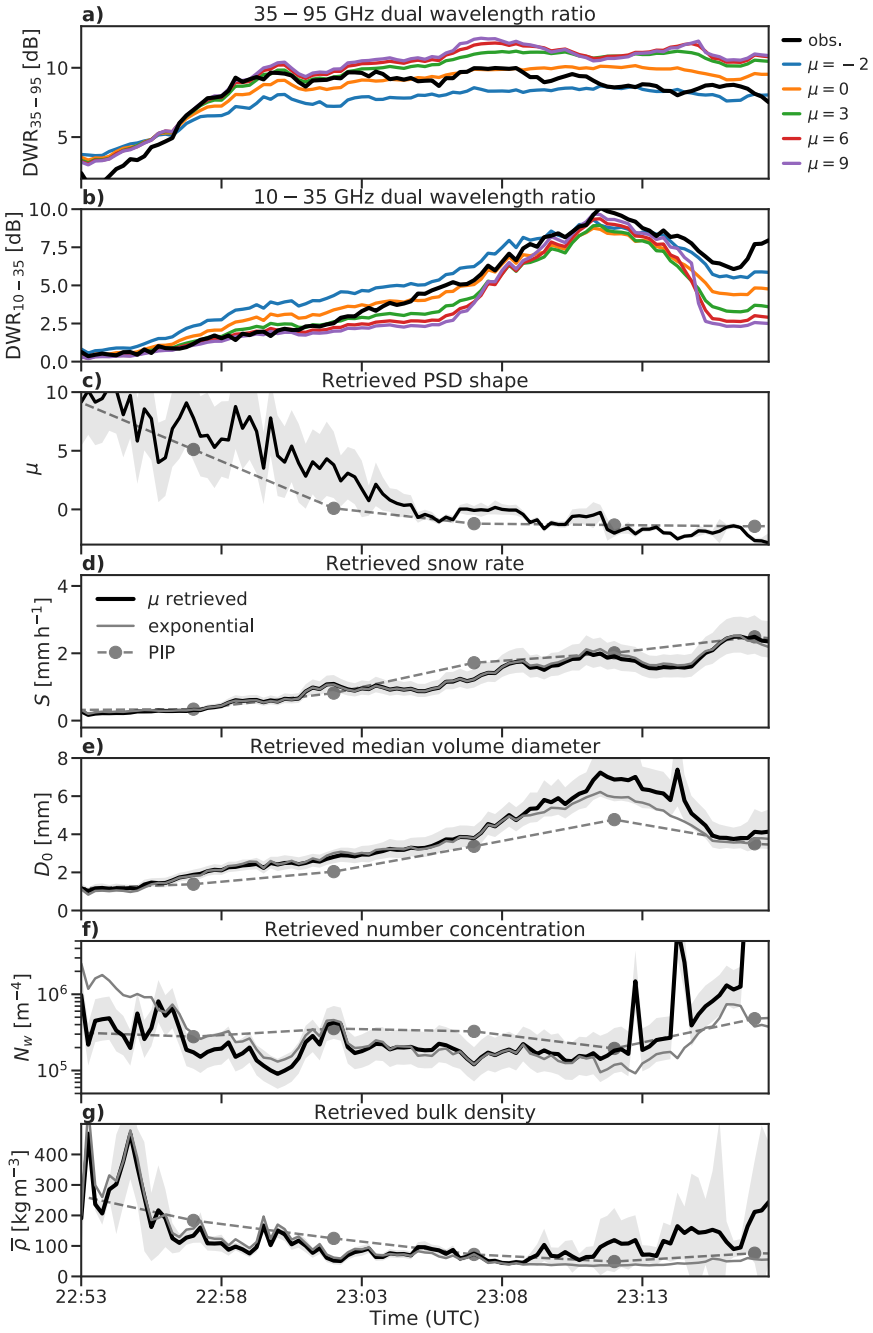

Figure 10. Measured and forward-modelled (a) DWR_{35-95} and (b) DWR_{10-35} at 500 m above ground level for CAPTIVATE retrievals assuming a range of PSD types; (c) the retrieved PSD shape parameter compared against that estimated from in situ measurements at the surface by PIP; and (d) snow rate, (e) median volume diameter, (f) normalised number concentration, and (g) bulk density comparing values for the pseudo-retrieval against one in which exponential PSDs are assumed. Shaded regions represent the uncertainty in the retrieved values.

~~which~~ where non-Rayleigh scattering is ~~insignificant at 95-GHz. Comparison to the PSD shape~~ weak at all frequencies. As a result, triple-frequency radar signatures using 95, 35 & 10 GHz frequencies provide little insight into ice or snow with median volume diameters below 2 mm. It has been suggested that the inclusion of G-band radars (e.g. 140 or 220 GHz) would provide additional insights into smaller ice particles [*Battaglia et* al., 2014]. Comparison of the retrieval to PSD shape parameters estimated from PIP measurements is especially difficult when ~~snow is dominated by small particles, where truncation effects on the use of the method of moments to estimate~~ the PSD has a median volume diameter below around 1 mm, whereupon disdrometer truncation has a significant effect on estimates of the parameters of the PSD ~~become significant~~from the method of moments [*Moisseev and Chandrasekar*, 2007].

The ~~triple-frequency~~ retrievals of snow rate, median volume diameter, number concentration and bulk density at 500 m are all reasonably well-matched to in situ measurements at the surface, given the differences in temporal resolution between the two estimates. The ~~snow rate is very similar to that measured at the surface, while the median volume diameters are~~ median volume diameter is overestimated by around 50 % in the period of heaviest ~~frontal snowfall, and~~ unrimed snowfall, while retrieved normalized number concentration is within a factor of two of the PIP estimates. While retrieving ~~PSD shape~~ the PSD shape parameter enables a significant improvement in the representation of triple-frequency radar measurements, we note that ~~this~~ it has little impact on the retrieved snow rate or bulk density when compared to a retrieval that assumes an exponential PSD. ~~Retrieving a~~ Compared to a retrieval assuming an exponential PSD, retrieving a broad PSD in the ~~frontal~~ unrimed snowfall results in median volume diameters roughly 1 mm ~~greater;~~ larger, while normalised number concentrations are as much as a factor of two lower in the ~~prefrontal regime ,~~ rimed regime and up to a factor of two greater toward the end of the ~~frontal regime.~~ unrimed regime.

5 The effect of aggregate internal structure: 16 February 2014 case study

~~It has been well established in numerical and experimental studies~~

In Section 3 we showed that the triple-frequency radar signature of snow ~~can provide insights into the structure, size and density of ice particles~~is sensitive to the density factor and internal structure of snowflakes, and also to the shape parameter of the PSD. In Section 4 values of density factor corresponding to riming were constrained by Doppler velocity measurements, while the transition in particle structure between aggregates of bullet rosettes for unrimed snow and homogeneous spheroids for graupel was parameterised by the density factor. This allowed variations in the PSD shape parameter to be constrained from triple-frequency radar reflectivity factors. In this section we consider a case in which the internal structure of unrimed snow varies due to the aggregation of different monomer particles.

Between 00:00 and 01:00 UTC on 16 February 2014 (Fig. 5) a light snowfall between 0.5 and 1.5 $\mathrm{m\,s^{-1}}$ was measured at Hyytiälä [~~*Kneifel et* al., 2011; *Leinonen et* al., 2012;~~ see Section 3.3.1 of *Kneifel et al.*, 2015~~; *Stein et* al., 2015~~, for a more detailed discussion of the meteorology]. ~~Triple-frequency radar studies~~ Generating cells are evident in radar reflectivity and DWR above around 4 km or −20 °C; below this level fall streaks indicate that precipitating ice is subject to strong winds down to around 2.5 km or −8 °C. Between −8 and −5 °C rapid increases in radar reflectivity and $\mathrm{DWR_{35-95}}$ are evident; this

temperature range is conducive to rime splintering [~~with the exception of *Leinonen et* al., 2012~~*Hallett and Mossop*, 1974] ~~have typically assumed exponential size distributions—an assumption also commonly made in radar retrievals because uncertainties in the PSD shape have a relatively weak influence on estimates of ice water content~~ and to the growth of needles [~~e.g.~~*Delanoë*, ~~2005~~Fig. 7 of *Kneifel et* al., 2015, shows that this temperature range is supersaturated with respect to ice]. *Kneifel et* al. [2015] showed (their Fig. 10) that when the snowfall was dominated by aggregates with very open structures, measured triple-frequency radar signatures exhibited maximum DWR_{35-95} values of around 6 dB, which is significantly weaker than expected for the triple-frequency radar signatures of most aggregates, but consistent with aggregates of large needles [Fig. 3e in *Leinonen and Moisseev*, 201 and Fig. 3 herein]. ~~In this study, we have shown that the PSD shape has an important effect on the~~ *Sinclair et* al. [2016] used the polarimetric signatures from a nearby scanning radar and a clustering analysis on PIP observations to argue that the snow at the surface comprised a mixture of graupel and small needles—the primary and secondary ice the Hallett-Mossop process—and large aggregates resulting from the rapid growth and aggregation of needles near the surface.

We first explore how the particle models developed in Section 3 can be used to account for the variability in triple-frequency radar signatures in this challenging case (Section 5.1), and we evaluate the effects of variations in ice particle internal structure on CAPTIVATE retrievals (Section 5.2).

5.1 Triple-frequency radar signatures

We separate the case into three snow regimes by comparing triple-frequency radar ~~signature by exaggerating or smoothing over features in the radar backscatter spectra,~~ measurements with the signatures forward-modelled for aggregates of needles, aggregates of bullet rosettes, and homogeneous spheroids. In forward-modelling the triple-frequency radar signatures we must also quantify the PSD shape parameter and density factor. PIP measurements indicate a broader than exponential PSD ($\mu = -1$) throughout the case, likely influenced by snowfall comprising distinct populations of large and small particles. Mean Doppler velocities around 1.5 m s−1 near the surface (Fig. 5d) indicate the radar measurements are dominated by unrimed particles ($r \approx 0$), except toward the end of the case where mean Doppler velocities approach 2 m s^{-1}, and more graupel is observed.

Triple-frequency radar measurements during the first regime (00:00 to 00:25 UTC; Fig. 12a) are most consistent with aggregates of bullet rosettes. Median volume diameters are up to 5 mm, with most between 1.5 and ~~that this influence can be more significant than changes in particle density. Using ground-based triple-frequency radar measurements alongside in situ measurements of particle properties~~ 3.5 mm; at the surface, ~~we showed that including variations in the PSD shape permitted more accurate representations of the measured~~ PIP measures $D_0 = 2.5$ mm (Fig 13c). The second regime (00:25 to 00:50 UTC; Fig. 12b) is characterised by the lower values of $\mathrm{DWR}_{35,95}$ associated with aggregates of needles. The triple-frequency measurements suggest median volume diameters up to 1 cm, with most between 3 and 4.5 mm, which is slightly higher than measured by PIP. The spread of the measurements lateral to the forward-modelled triple-frequency radar signatures ~~of graupel-like particles modelled as homogeneous spheroids, and of unrimed aggregate snowflakes modelled as fractals.~~

~~The potential to use advanced radar measurements to constrain ice particle properties in retrievals is of significant interest for reducing uncertainties in remote-sensed estimates of ice water content and snowfall, as well as improving understanding~~

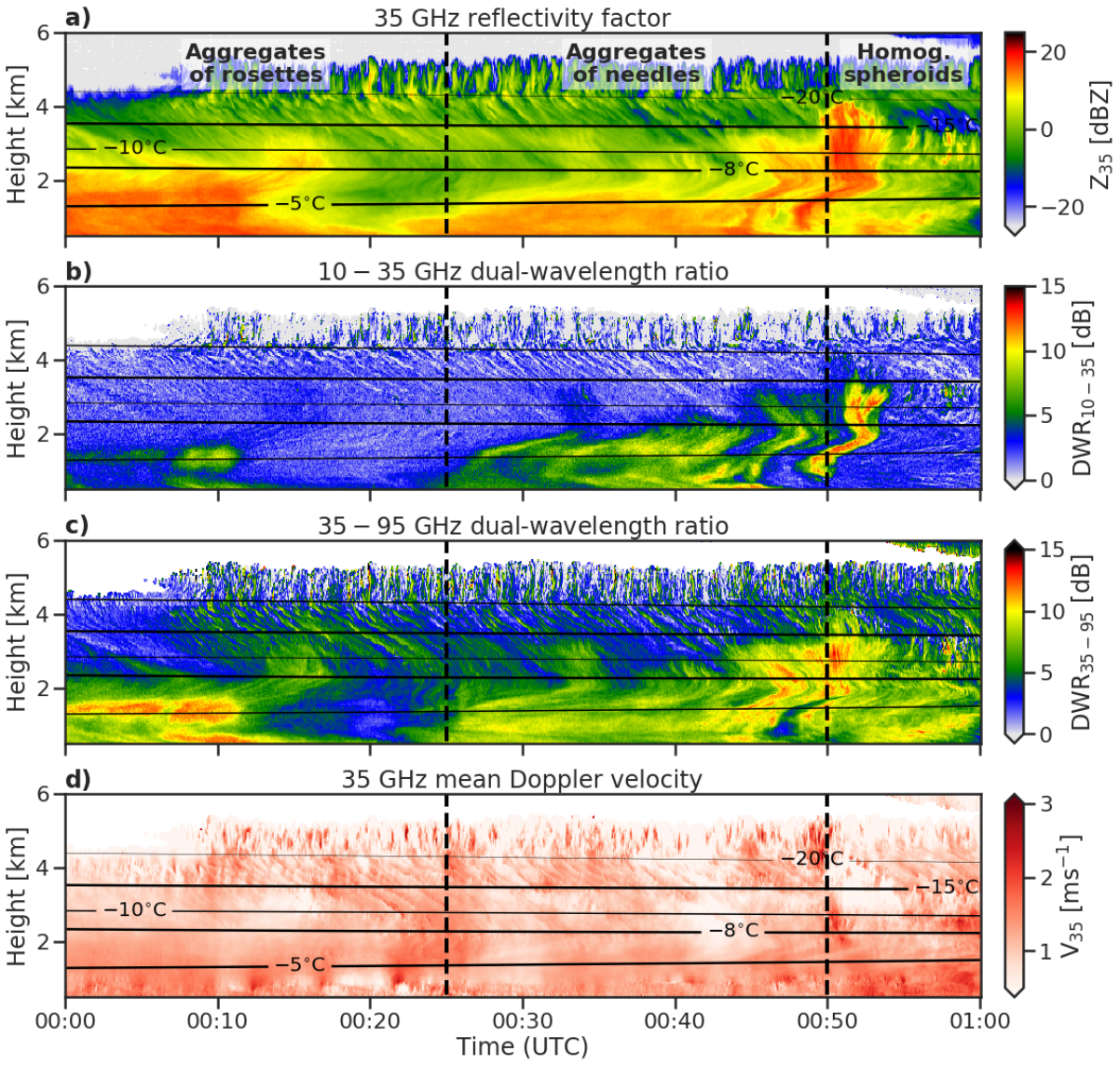

Figure 11. Triple-frequency Doppler radar measurements from the February 21 2014 case study at Hyytälä, Finland. (a) 35 GHz radar reflectivity, (b) 10–35 GHz dual wavelength ratio, (c) 35–95 GHz dual wavelength ratio, and (d) 35 GHz mean Doppler velocity. Vertical dashed lines mark the transition between the rimed and unrimed snowfall regimes; solid lines are contours of temperature from ECMWF analysis.

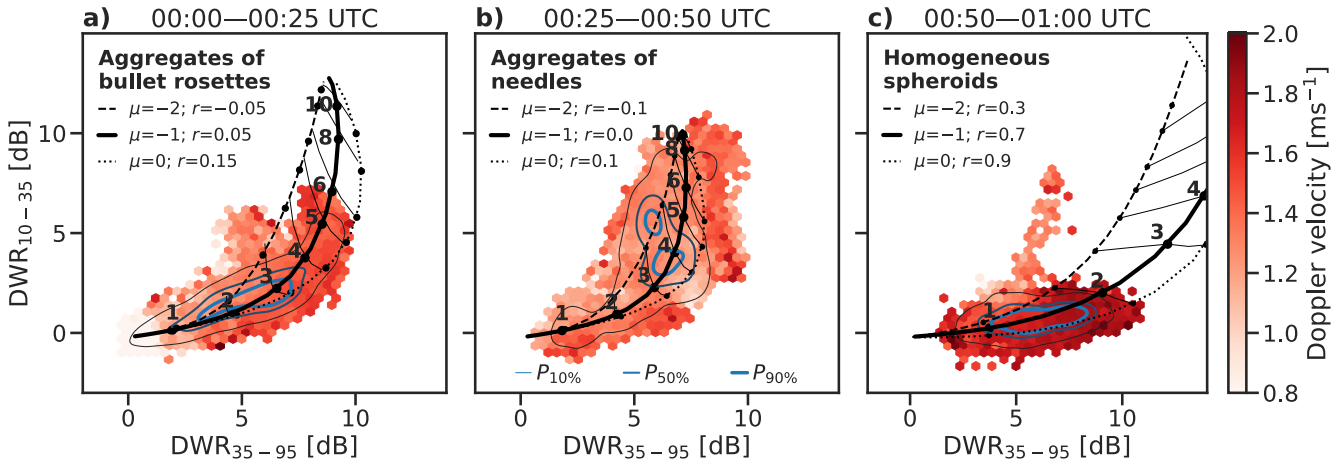

Figure 12. Triple frequency radar measurements from below 1 km above ground level during the 16 February case. The data are divided into three regimes and overlaid by a range of particle models, as informed by PIP measurements. Throughout this case a PSD shape parameter of $\mu = -1$ was measured in situ. (a) The period 00:00–00:25 UTC is consistent with the triple-frequency radar signature of aggregates of bullet rosettes (Table 1), (b) the period 00:25–00:50 UTC is to aggregates of needles (Table 1), and (c) the period 00:50–01:00 UTC to homogeneous spheroids. The triple-frequency radar measurements are coloured by the average mean Doppler velocity, and blue contours mark the 10th, 50th and 90th percentiles of the frequency of the data.

~~of~~ may be indicative of a particles with a range of internal structures within this regime, such as may result from aggregates from different sized needles. Toward the end of the snowfall event (00:50 to 01:00 UTC; Fig. 12 c) the flatter triple-frequency radar signature is consistent with small homogeneous spheroids with median volume diameters less than 2 mm. Relatively large density factors ($r > 0.5$) are required to match the dominant flat triple-frequency signature for such small particles. Some measurements with $\mathrm{DWR}_{10-35} > 3$ dB are a reminder that this regime includes a mixture of particle types, the ~~microphysics of ice and mixed-phase cloud. Two recent studies have used~~ triple-frequency ~~airborne radar measurements to constrain retrievals of ice particle density by modifying the prefactor of the mass-size distribution~~ radar signatures of which are consistent with a small amount of the aggregates of needles.

This indicates that the full range of triple-frequency radar measurements cannot be covered by transitioning between a single model for aggregate particles and homogeneous spheroids. The distinct internal structure of some particles, such as aggregates of needles, must also be represented. While these regimes and corresponding particle models are identified based on the measured triple-frequency signatures, we note that the snow falling throughout this event comprises a mixture of these particle types [~~*Leinonen et* al., 2018; *Tridon et* al., 2019~~*Sinclair et* al., 2016]~~; however, both studies found that~~. In the particle imagery shown in *Kneifel et* al. [2015] the largest aggregates of needles were sampled from 00:38 to 00:50 UTC, but graupel was also observed. Prior to 00:25 UTC the particle imagery shows both graupel and needles inter-mixed with large aggregates; finally, after 00:50 UTC, aggregates of needles are observed as well as graupel.

5.2 Triple frequency radar retrievals

We will now evaluate the capabilities and limitations of CAPTIVATE retrievals assuming a range of particle models. Unlike the February 21 case, PIP measurements indicate a broad PSD ($\mu = -1$) throughout this case; we therefore set $\mu = -1$ for all retrievals, acknowledging that this prior knowledge from in situ measurements is not always available for remotely-sensed estimates of snow. To consider the importance of resolving different particle structures, we carry out three retrievals, using each of the particle types considered in Section 3: aggregates of needles, aggregate of bullet rosettes, and homogeneous spheroids. In order to expand the range of triple-frequency ~~radar retrievals were not substantially different from dual-frequency retrievals, suggesting that the problem was over-constrained. An alternative approach to estimating ice particle properties has been to use Doppler velocity as a constraint on particle density *Szyrmer and Zawadzki*, 2014a; *Mason et* al., 2018. In this study we have built upon dual-frequency Doppler retrievalsusing the CAPTIVATE optimal estimation framework in which ice particle density, shape and microphysical structure are parameterized to represent a continuum of ice particles from unrimed aggregate snowflakes to dense graupel and hail *Mason et* al., 2018. To our knowledge the present study is the first demonstration of a triple-frequency Doppler radar retrieval of the properties of snow particles. We found that varying the PSD shape to fit that measured in situ allowed for a retrieval in which the profiles of~~ radar ~~reflectivity measured at all three frequencies could be accurately represented—that is , only when non-exponential PSDs were permitted did the state space include a solution that satisfied the radar measurements at all three frequencies. From an ensemble of retrievals assuming a range of PSD shapes, a pseudo-retrieval was made of~~ signatures represented, an additional distinction is made between aggregates of "large" and "small" needles, where the latter corresponds to the fit to aggregates of needles in Section 3, and the former takes a lower value of power-law exponent ($\gamma = 4/3$ instead of $\gamma = 5/3$); this is consistent with the relation of the ~~PSD shape that best fit the~~ triple-frequency radar signature to larger needle monomers observed by *Leinonen and Moisseev* [2015]. Unlike in the previous case, the hybrid approach transitioning between aggregates of bullet rosettes at low density factors and homogeneous spheroids at high density factors is not used. As such, we cannot expect any one retrieval to accurately represent the entire case, and it may be that we are unable to adequately resolve the features of snow known to comprise a mixture of different particle types. Nevertheless, by comparing these retrievals we hope to show how effectively variations in the internal structure of ice particles may improve the fit to triple-frequency radar measurements~~. This yielded an estimate of PSD shape, ~~, and also how sensitive the retrieved quantities are to different particle models.

The forward-modelled dual-frequency ratios (Fig. 13a & b) show how well-constrained each retrieval is by the observed variables. PIP measurements of the PSD shape parameter and the constant assumption of $\mu = -1$ are compared in Fig. 13c, and Fig. 13d–g show the retrieved estimates and PIP measurements of snow rate, median volume diameter~~and ~~, normalized number concentration ~~which compared well with in situ measurements at the surface; however, more accurate estimates of PSD shape had only aweak effect on the~~ and bulk density.

The spread in forward-modelled DWRs are as much as 3 dB when the measured DWRs are large; however, when the measured DWR is low (i.e. toward the lower-left part of the triple-frequency radar signature diagram) the retrievals are almost insensitive to the particle model. The maximum values of DWR_{35-95} (Fig. 13a) are indicative of the maximum extent of

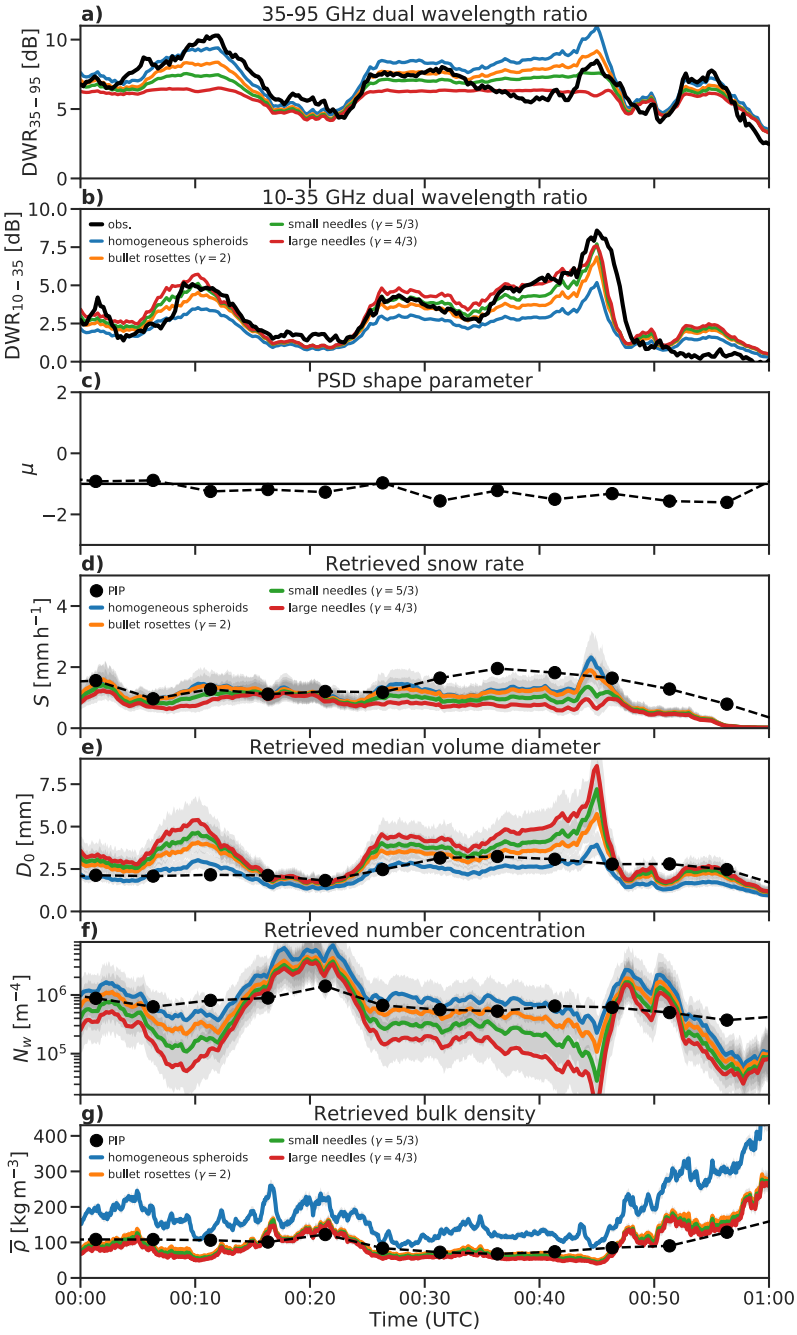

Figure 13. Triple-frequency Doppler radar retrievals from the 16 February 2014 case during BAECC, assuming homogeneous spheroids, aggregates of bullet rosettes, and aggregates of large and small needles. The forward-modelled 35-94 GHZ (a) and 10-35 GHx (b) dual-frequency ratios are compared against radar measurements. The assumed PSD shape parameter $\mu = 1$ for all the retrievals reflects the near-constant in situ measurements throughout the case (c). The retrieved snow rate (d), median volume diameter (e), normalized number concentration (f) and bulk density (g) at 500 m above ground level are compared against PIP measurements at the surface.

the hook feature of the triple-frequency diagram: accordingly, the aggregates of needles have the lowest maximum values, saturating around 6 or 7 dB. Conversely, the lowest values of DWR_{10-35} (Fig. 13) correspond to homogeneous spheroids, while the greatest are for the aggregates of needles. The retrieved snow rate ~~when compared with retrievals assuming an exponential PSD. Furthermore, even when the PSD shape was well-represented, triple-frequency radar measurementsdid not provide an adequate constraint on the density of ice particles compared with that provided by mean Doppler velocity. This supports the approach of combining Doppler and multiple-frequency radar measurements~~ is sensitive to particle structure with differences of 0.5 to ~~most thoroughly characterise both the size distribution and morphology of ice particles~~ 1 mm h^{-1} between aggregates of large needles and homogeneous spheroids, except where the measured DWR are lowest. The estimates of median volume diameter and normalized number concentration assuming homogeneous spheroids are closer to the PIP measurements than the estimates assuming aggregate snowflakes. However, when homogeneous spheroids are assumed the bulk density is overestimated by around 100 % with respect to PIP measurements.

While the triple-frequency radar signatures of the three regimes were broadly represented by three different particle types, the time series shows much more variability. In the first regime (00:00–00:25 UTC), the triple-frequency radar signature of which was a fit to aggregates of bullet rosettes, DWR_{35-95} takes large values associated with graupel, while DWR_{10-35} jumps between values consistent with graupel and the larger ratios more characteristic of aggregates. These fluctuations are likely due to the mixture of different particle types. The second regime (00:25–00:50 UTC) is a more consistent fit to aggregates of needles: between 00:25 to 00:35 UTC the measurements correspond to aggregates of small needles, while between 00:35 to 00:45 UTC—where the lowest values of $DWR_{35-95} \approx 6$ dB are observed—the aggregates of larger needles offer a good fit to measurements. While the aggregates of needles dominate the triple-frequency radar signature, this regime is associated with the greatest errors in retrieved snow rate, which is roughly half that of the PIP retrieval, in conjunction with lower normalized number concentrations and much larger median volume diameters. It seems likely that, due to CAPTIVATE assuming a single population of particles and being constrained by the largest particles, the contribution of graupel to the snow rate is being disregarded. Finally, after 00:50 UTC DWR_{10-35} decreases to less than 3 dB, consistent with compact graupel-like particles. The differences between retrievals are relatively small in this regime: all tend to underestimate the snow rate compared to PIP, but correctly resolve the increase in bulk density.

The ~~sensitivity of~~ range of forward-modelled DWRs for retrievals assuming particles with different internal structures are as much as 3 dB. As observed in the triple-frequency radar signatures~~to the shape of the PSD suggests a need to represent non-exponential PSDs within multiple-radar retrievals, but the importance of spectral features to~~ , this is of a similar magnitude to the variations due to uncertainties in the density and PSD shape. Unlike the PSD shape parameter, uncertainty in particle structure results in a spread in retrieved snow rates. This case includes both rime splintering and rapid aggregation of secondary ice particles, leading to snowfall at the surface comprising compact graupel, needles, and large aggregates of needles. Secondary ice poses a challenge for radar retrievals. The triple-frequency radar ~~measurements may also require an evaluation of the suitability of the Gamma distribution for representing PSDs. The shape factor of the Gamma PSD provides a convenient means of modifying the width of the PSD; however, in situ measurements of ice clouds have supported the use of modified distributions to allow for more complex size spectra~~ signatures are dominated by the largest particles, which are slow-falling aggregates.

Assuming this particle type within the retrieval neglects compact and fast-falling graupel, leading to an underestimate of the snowfall at the surface. Conversely, assuming homogeneous spheroids for the retrieval results in a better fit to the snow rate, but the retrieval significantly over-estimates bulk density and is poorly constrained by the triple-frequency radar reflectivity factors.

6 Discussion and conclusions

It has been well-established in theoretical and observational studies that triple-frequency radar measurements of snow can provide insights into the microphysical structure and density of ice particles [*Kneifel et* al., 2011; *Leinonen et* al., 2012; *Kneifel et* al., 2015; *Stein et* al., 2015]. In the context of recent ground-based [e.g. ~~*Delanoë*, 2005; *Field et al.*, 2005, 2007~~*Petä*, 2016] ~~, which can also be implemented within CAPTIVATE~~ and airborne [~~*Mason et* al., 2018~~e.g. *Houze et* al., 2017] multiple-frequency radar measurements, large databases of realistic ice particles from numerical simulations and in situ measurements are being used to better understand the links between ice microphysics and multiple-frequency radar scattering properties [*Kneifel et* al., 2018]. One important application of this research is to assimilate triple-frequency radar measurements in radar retrievals that estimate variations in ice particle properties, such as due to riming [*Leinonen et* al., 2018a; *Tridon et* al., 2019]. ~~In a recent study, *Grecu et* al. [2018] demonstrated a retrieval of ice water content and median diameter from airborne~~ A significant challenge in developing this capability is to sufficiently represent the parameters that influence the triple-frequency ~~radars in which the estimation was informed by a database of PSDs measured in situ, rather than assuming parameterised PSDs. Consistent with the findings of the present study, they found that including natural variability in particle spectra resulted in greater ambiguity between the~~ radar signature in order to either estimate them within retrievals, or to quantify their contributions to retrieval uncertainties.

We began this study by using approximations to radar backscatter cross-section of ice particles to explore the parameters that most strongly affect their triple-frequency ~~radar signatures of different particle typesthan may be expected from studies assuming exponential PSDs for all~~ radar signatures. The triple-frequency radar signature varies due to both the density and homogeneity of ice particles, consistent with the conceptual model of *Kneifel et* al. [2015]. For aggregate particles represented by the self-similar Rayleigh-Gans approximation [SSRGA; *Hogan et* al., 2017], the magnitude and scale-dependence of random fluctuations in internal structure are also important, as explored by *Stein et* al. [2015] and *Leinonen and Moisseev* [2015]. The SSRGA provides physically meaningful parameters by which both the shape of the average particle, and the small-scale fluctuations in the structure represented by a power spectrum, can be tuned. To inform our interpretation, we fit SSRGA coefficients to simulated aggregates of a range of monomer types, and showed that aggregates of needles have a distinct triple-frequency radar signature from aggregates of other particles [~~e.g. *Kneifel et* al., 2011; *Leinonen and Szyrmer*, 2015~~see also *Leinonen and Moisseev*, 2015]. Finally, while most radar studies of snow assume exponential PSDs, we showed that the PSD shape parameter has a similar effect on triple-frequency radar measurements to particle density by modifying the relative importance of features in the radar backscatter spectrum. Next, we used radar and in situ measurements of snow to disentangle the multiple parameters affecting observed triple-frequency radar signatures.

~~Joint histograms of (a) snow rate, (b) median volume diameter, (c) normalized number concentration and (d) bulk density against PSD shape μ from 2 years of PIP observations taken at Hyytiälä, Finland *von Lerber et* al., 2017. Solid black lines mark the median of the respective quantities for each value of PSD shape; dashed lines mark the 10th and 90th percentiles of the distribution.~~

~~We have made a remotely-sensed estimate of~~ We evaluated our particle models against triple-frequency radar measurements and particle properties from in situ observations of two snow events from the BAECC 2014 field campaign at Hyytiälä, Finland [*Kneifel et* al., 2015]. First we applied information from particle imaging measurements to select the particle model that best represents the triple-frequency radar signature for each snow regime. In a case including heavily rimed graupel and unrimed aggregates, the triple-frequency radar signature of graupel was consistent with homogeneous spheroids with a moderate density factor and a narrow PSD, while the large unrimed aggregates were represented by aggregates of bullet rosettes with a broad PSD. In a contrasting case including the production and rapid aggregation of secondary ice particles due to rime splintering, triple-frequency signatures were indicative of a mixture of unrimed aggregates of bullet rosettes and aggregates of needles, and of heavily rimed compact graupel particles. Based on in situ measurements during this case, significant fluctuations in the triple-frequency radar signature can be confidently attributed to the internal structure of the aggregates, rather than to changes in the PSD shape ~~using a pseudo-retrieval that minimises the error in~~ or particle density.

Based on these insights, we sought to better understand how the density and internal structure of particles, and the PSD shape parameter, can be included or accounted for in triple-frequency ~~radar measurements from an ensemble of retrievals; however, future work should focus on expanding the state space to include the PSD shape within the optimal estimation framework. CAPTIVATE has been developed for retrievals from the EarthCARE 94-GHz Doppler cloud profiling radar in synergy with lidar and radiometers~~ radar retrievals. We ran a range of CAPTIVATE [~~*Illingworth et* al., 2015, and while it provides the flexibility to assimilate measurements from multiple radars and modify the state vector to parameterise ice particle properties, PSD shape is not currently configurable as a state variable. Retrieving PSDshape within the optimal estimation framework would have the advantages of permitting an a priori assumption of exponential PSDs when triple-frequency measurements provide little information, of quantifying uncertainties in the retrieved PSD shape , and of allowing changes in PSD shape to be resolved through the profile. Estimates of all three parameters of a Gamma PSD and their associated uncertainties would contribute to studies using advanced remote sensing to better observe the relationship between particle properties and microphysical processes *Mace and Benson*, 2017; *Mason et al.*, 2018] .~~

~~In the present configuration of CAPTIVATE it was found that~~ retrievals for each case, and compared remotely-sensed estimates to PIP measurements at the surface. In the case including graupel and unrimed aggregates, we demonstrated that the assumption of an exponential PSD resulted in triple-frequency radar ~~measurements could be used to retrieve three parameters of the PSD, but they were a relatively weak constraint on the density, shape and structure of the ice particles—the parameterisation of which was formulated to be constrained by Doppler velocity information~~ retrievals that were over-constrained. Only when non-exponential PSDs were assumed, informed by PIP measurements, was the retrieval able to satisfy all three radar reflectivity factors. Further, we found that while the mean Doppler velocity can be exploited to estimate both the density factor and the transition between aggregate snowflakes and homogeneous graupel particles [as in *Mason et al.*, 2018]~~. The~~

~~low sensitivity of the retrieved particle density to~~ , the density factor was not well-constrained by triple-frequency radar ~~measurements may be because the rimed snow in this case comprised compact graupel-like particles with median volume diameters near the limit for the onset of non-Rayleigh scattering at 95-GHz. Given the well-established links between particle morphology and~~ reflectivity factors. This is consistent with *Leinonen et* al. [2018a], who found the prefactor of the particle mass-size relation was insensitive to the assimilation of a third radar frequency. However, the third radar frequency proved essential to constraining the median volume diameter of aggregate snowflakes: due to the characteristic hook feature of their triple-frequency ~~measurements, the use of triple-frequency radar signatures to retrieve ice particle properties should not be ruled out; retrievals of cases featuring the riming of larger aggregates may find that the triple-frequency~~ radar ~~measurements provide a stronger constraint on particle density. In the case studied here there is a strong association between PSD shape and particle morphology, with the prefrontal regime characterised by a narrow distribution of graupel-like particles~~signature, DWR_{35-95} becomes saturated at values around 7 to 10 dB, and provides little information on the size of large aggregates. Next we demonstrated a novel approach to use the third radar reflectivity factor to estimate the PSD shape parameter. This pseudo-retrieval was made by minimising errors in DWRs from an ensemble of retrievals assuming a range of PSD shape parameters, and the ~~frontal regime by a broad PSD dominated by large aggregate snowflakes. Two winters of the properties of snow at Hyytiälä from the retrieval of *von Lerber et* al. [2017] show that narrower PSDs are consistently associated with light snowfall dominated by smaller and denser particles, while broad PSDs are associated with the heaviest snowfall and dominated by large, low-density snowflakes. The tendency of heavily rimed snow and graupel to have narrower size distributions~~ result compared well with PIP measurements at the surface. Accounting for variations in the PSD shape parameter is necessary to assimilate triple-frequency radar reflectivity factors, and retrievals of the PSD shape parameter may provide insights into microphysical processes in snow. In the case of heavy riming studied here, narrow PSDs were strongly correlated with riming and broad PSDs with aggregation; while this is consistent with some other observations [*Garrett et al.*, 2015]~~; however,~~ , we note that *Tiira et al.* [2016] found only a weak relation between ~~ice bulk density and PSD shape measured at Hyytiälä. Some studies have linked PSD shape to median volume diameter or a spectral width parameter~~ bulk ice density and the PSD shape parameter measured during BAECC, and we anticipate further research associating PSD shape with aggregation and riming processes in snow. An important result, however, is that varying the PSD shape parameter does not significantly change the retrieved snow rate, justifying the common assumption of exponential PSDs for single- and dual-frequency radar retrievals [~~*Williams et* al., 2014, a method which may be especially suited to studies combining triple-frequency and Doppler spectral information *Kneifel et* al., 2016~~*Delanoë*, 2005]~~; however, correlations between PSD parameters measured by distrometers must be treated with caution due to~~ . Nevertheless, the capability to remotely-sense changes in the PSD shape parameter alongside other properties of snow may provide significant insights into processes of aggregation and riming in snow.

Retrievals of the second case study focused on the importance of the internal structure of aggregate snowflakes. In this case the PSD shape parameter at the surface was near-constant. While the presence of graupel was evident in the particle imaging measurements and is necessary for the rime splintering process, the triple-frequency radar signatures were dominated by large aggregates. CAPTIVATE retrievals of this case assumed a range of different particle structures from homogeneous spheroids to aggregates of large needles. In the regime where the largest aggregates of needles were observed at the surface,

the retrieval assuming these particles was best able to represent the assimilated triple-frequency radar measurements; however, this corresponded to an significant underestimate of surface snow rate. Conversely, assuming graupel-like particles resulted in a weak fit to the assimilated measurements but a better representation of surface snowfall. This illustrates the challenges of secondary ice production to radar retrievals, wherein a single particle population is typically assumed: because the radar measurements are dominated by the largest aggregates, the contribution of dense, fast-falling graupel particles to the ~~possibility of statistical artefacts due to spectral truncation *Moisseev and Chandrasekar*, 2007. Further in situ measurements from a variety of locations are needed to study the processes linking PSD shape with particle morphology, and will be critical to maximising the use of~~ snowfall is neglected in the retrieval. Unlike the PSD shape parameter, variations in particle internal structure contribute significant uncertainties in the retrieved snow rate; however, we note that aggregates of most monomers appear to exhibit broadly similar triple-frequency radar signatures~~in retrievals~~, to which aggregates of large needles are an exception. It is not clear how frequently biases in radar retrievals due to these effects may be expected to affect snowfall estimates; however, the ranges of temperatures at which these occur are well understood [e.g. *Korolev et* al., 2000; *Heymsfield et* al., 2013].

~~We have demonstrated a novel method using~~ We have identified a number of parameters that affect the triple-frequency ~~Doppler radar measurements from the snow experiment intensive observation period of the BAECC~~ radar signature of snow and should therefore be considered within triple-frequency radar retrievals. Two short case studies have been used to demonstrate contrasting situations in which the effects of these parameters, as represented within models for the size distribution, morphology and radar backscatter cross-section of ice particles, can be observed in radar measurements and affect radar retrievals of snowfall. Particle density and the transition from aggregate snowflakes to more homogeneous graupel particles, which are inter-related in the riming process, have dominated the conceptual model explaining the triple-frequency radar signature [*Kneifel et* al., 2015], and were included in the retrieval of *Mason et* al. [2018]. The PSD shape parameter has usually been excluded from studies of the triple-frequency radar signature by assuming an exponential PSD, an assumption which is justified in radar retrievals in many situations by the weak effect of the PSD shape parameter on the snow rate. However, the influence of the PSD on the triple-frequency radar signature is similar in magnitude and sense to that of the density factor, and misinterpretation of triple-frequency radar data may result if both parameters are not accounted for. In a recent study, *Grecu et* al. [2018] demonstrated retrievals from airborne triple-frequency radars informed by PSDs measured in situ, rather than assuming parameterised PSDs. Consistent with the present study, they found that including variability in particle spectra resulted in greater ambiguity between the triple-frequency radar signatures of different particle types than may be expected from studies assuming exponential PSDs for all particles [e.g. *Kneifel et* al., 2011; *Leinonen and Szyrmer*, 2015]. While the density factor and the transition from aggregates to homogeneous spheroids are represented, the PSD shape parameter and variations in the internal structure of aggregate snowflakes are not currently implemented as state variables within CAPTIVATE. Including such parameters in the radar forward model would allow for information about their natural variability to be propagated into the uncertainties of retrieved quantities. If adequately constrained by radar and synergistic measurements, some parameters such as the PSD shape parameter may be retrieved. The challenges of quantifying both secondary ice and variations in the PSD may be best addressed using Doppler spectra [e.g. *Kneifel et* al., 2016], and this should be the subject of future work.

Two case studies from BAECC 2014 ~~campaign in Hyytiälä, Finland. The simultaneous retrieval of the~~ at HyytiÏä, Finland, have been used to demonstrated the impact of particle size distribution and ~~morphology of ice particles is only possible due to the availability of~~ internal structure to triple-frequency radar measurements, but further work is needed to establish the relative importance of variations in these parameters to estimates of global snowfall. The evaluation of triple-frequency Doppler radar retrievals against in situ particle properties depends on high-quality remotely-sensed measurements supported by in situ observations at the surface [*Tiira et al.*, 2016; *von Lerber et al.*, 2017; *Moisseev et al.*, 2017] ~~, and~~ in a location where wintertime precipitation is frequently not affected by melting. The significant challenges of colocating and cross-calibrating multiple radars ~~, and of~~ and correcting for attenuation due to supercooled liquid ~~water, have been addressed by *Kneifel et* al. [2015]; any of these effects have the potential to introduce significant~~ water—any of which are potential biases and uncertainties in the ~~retrieval, reinforcing the need for high quality in situ measurements. The~~ present retrieval—have been addressed by *Kneifel et* al. [2015] and *Dias Neto et* al. [2019]. The general scarcity of such high quality datasets ~~,~~ and their importance for evaluating our models of ice particle morphology and size distribution, and for testing retrievals against in situ measurements, make the case for further and ongoing deployments of multiple-frequency Doppler radar instruments at a range of ARM and Cloudnet field sites. Increasing the geographic diversity of ground-based snow studies, as well as the quantity of measurements, will be critical to increasing confidence in the use of models of ice particles and microphysical processes for global snowfall estimates.

~~Insights~~ In addition to developing the capability for more advanced radar retrievals, insights into ice and mixed-phase microphysics ~~triple-frequency Doppler radar retrievals may inform~~ from multiple-frequency and Doppler radar measurements of snow should be focused on informing the ice particle models used in ~~retrievals with fewer radar frequencies, such as to the 94-GHz~~ other radar retrievals, and especially snowfall estimates from spaceborne radars such as the 94 GHz Doppler cloud profile radar aboard EarthCARE [*Illingworth et al.*, 2015]. The present work contributes to a more detailed understanding of the uncertainties of radar retrievals due to variations in the properties of snow. In planning for satellite missions beyond EarthCARE [*Engineering and Medicine*, 2018], the benefits of dual-frequency radar as a constraint on the size and number concentration of hydrometeors has been well-established ~~e.g. *Leinonen et* al., 2018; *Mason et al.*, 2017, 2018. As a constraint on the retrieval of particle density, triple-frequency radar has thus far provided relatively small advantages over dual-frequency radars *Leinonen et* al., 2018; *Tridon et* al., 2019when compared with Doppler velocity *Mason et* al., 2018; however, ~~; here, we have demonstrated that triple-frequency radar measurements ~~can~~ may be used to constrain additional properties of the ~~PSD~~ morphology and size distribution of snow, to provide insights into ice and mixed-phase cloud microphysics.

References

Barrett, A. I., Westbrook, C. D., Nicol, J. C., and Stein, T. H. M.: Rapid ice aggregation process revealed through triple-wavelength Doppler spectrum radar analysis, Atmospheric Chemistry and Physics, 19, 5753–5769, https://doi.org/10.5194/acp-19-5753-2019, https://www.atmos-chem-phys.net/19/5753/2019/, 2019.

Battaglia, A. and Delanoë, J.: Synergies and complementarities of CloudSat-CALIPSO snow observations, Journal of Geophysical Research: Atmospheres, 118, 721–731, https://doi.org/10.1029/2012JD018092, http://doi.wiley.com/10.1029/2012JD018092, 2013.

Battaglia, A., Westbrook, C. D., Kneifel, S., Kollias, P., Humpage, N., Löhnert, U., Tyynelä, J., and Petty, G. W.: G band atmospheric radars: new frontiers in cloud physics, Atmospheric Measurement Techniques, 7, 1527–1546, https://doi.org/10.5194/amt-7-1527-2014, http://www.atmos-meas-tech.net/7/1527/2014/amt-7-1527-2014.htmlhttp://www.atmos-meas-tech.net/7/1527/2014/, 2014.

Brown, P. R. A. and Francis, P. N.: Improved Measurements of the Ice Water Content in Cirrus Using a Total-Water Probe, Journal of Atmospheric and Oceanic Technology, 12, 410–414, 1995.

Delanoë, J., Protat, A., Testud, J., Bouniol, D., Heymsfield, A. J., Bansemer, A., Brown, P. R. A., and Forbes, R. M.: Statistical properties of the normalized ice particle size distribution, Journal of Geophysical Research, 110, D10 201, https://doi.org/10.1029/2004JD005405, http://doi.wiley.com/10.1029/2004JD005405, 2005.

Delanoë, J. M. E. and Hogan, R. J.: A variational scheme for retrieving ice cloud properties from combined radar, lidar, and infrared radiometer, Journal of Geophysical Research, 113, D07 204, https://doi.org/10.1029/2007JD009000, http://onlinelibrary.wiley.com/doi/10.1029/2007JD009000/fullhttp://doi.wiley.com/10.1029/2007JD009000, 2008.

Dias Neto, J., Kneifel, S., Ori, D., Trömel, S., Handwerker, J., Bohn, B., Hermes, N., Mühlbauer, K., Lenefer, M., and Simmer, C.: The TRIple-frequency and Polarimetric radar Experiment for improving process observations of winter precipitation, Earth System Science Data, 11, 845–863, https://doi.org/10.5194/essd-11-845-2019, https://www.earth-syst-sci-data.net/11/845/2019/, 2019.

Field, P. R., Hogan, R. J., Brown, P. R. A., Illingworth, A. J., Choularton, T. W., and Cotton, R. J.: Parametrization of ice-particle size distributions for mid-latitude stratiform cloud, Quarterly Journal of the Royal Meteorological Society, 131, 1997–2017, https://doi.org/10.1256/qj.04.134, http://doi.wiley.com/10.1256/qj.04.134, 2005.

Field, P. R., Heymsfield, A. J., and Bansemer, A.: Snow Size Distribution Parameterization for Midlatitude and Tropical Ice Clouds, Journal of the Atmospheric Sciences, 64, 4346–4365, https://doi.org/10.1175/2007JAS2344.1, http://journals.ametsoc.org/doi/abs/10.1175/2007JAS2344.1, 2007.

Garrett, T. J., Yuter, S. E., Fallgatter, C., Shkurko, K., Rhodes, S. R., and Endries, J. L.: Orientations and aspect ratios of falling snow, Geophysical Research Letters, 42, 4617–4622, https://doi.org/10.1002/2015GL064040, http://doi.wiley.com/10.1002/2015GL064040, 2015.

Grazioli, J., Lloyd, G., Panziera, L., Hoyle, C. R., Connolly, P. J., Henneberger, J., and Berne, A.: Polarimetric radar and in situ observations of riming and snowfall microphysics during CLACE 2014, Atmospheric Chemistry and Physics, 15, 13 787–13 802, https://doi.org/10.5194/acp-15-13787-2015, http://www.atmos-chem-phys.net/15/13787/2015/, 2015.

Grecu, M., Tian, L., Heymsfield, G. M., Tokay, A., Olson, W. S., Heymsfield, A. J., and Bansemer, A.: Nonparametric Methodology to Estimate Precipitating Ice from Multiple-Frequency Radar Reflectivity Observations, Journal of Applied Meteorology and Climatology, 57, 2605–2622, https://doi.org/10.1175/JAMC-D-18-0036.1, http://journals.ametsoc.org/doi/10.1175/JAMC-D-18-0036.1, 2018.

Hallett, J. and Mossop, S. C.: Production of secondary ice particles during the riming process, Nature, 249, 26–28, https://doi.org/10.1038/249026a0, http://www.nature.com/articles/249026a0, 1974.

Hogan, R. J.: A Variational Scheme for Retrieving Rainfall Rate and Hail Reflectivity Fraction from Polarization Radar, Journal of Applied Meteorology and Climatology, 46, 1544–1564, https://doi.org/10.1175/JAM2550.1, http://journals.ametsoc.org/doi/abs/10.1175/JAM2550.1http://journals.ametsoc.org/doi/abs/10.1175/JAM2550.1, 2007.

Hogan, R. J. and Westbrook, C. D.: Equation for the Microwave Backscatter Cross Section of Aggregate Snowflakes Using the Self-Similar Rayleigh-Gans Approximation, Journal of the Atmospheric Sciences, 71, 3292–3301, https://doi.org/10.1175/JAS-D-13-0347.1, http://journals.ametsoc.org/doi/abs/10.1175/JAS-D-13-0347.1, 2014.

Hogan, R. J., Tian, L., Brown, P. R. A., Westbrook, C. D., Heymsfield, A. J., and Eastment, J. D.: Radar Scattering from Ice Aggregates Using the Horizontally Aligned Oblate Spheroid Approximation, Journal of Applied Meteorology and Climatology, 51, 655–671, https://doi.org/10.1175/JAMC-D-11-074.1, http://journals.ametsoc.org/doi/abs/10.1175/JAMC-D-11-074.1, 2012.

Hogan, R. J., Honeyager, R., Tyynelä, J., and Kneifel, S.: Calculating the millimetre-wave scattering phase function of snowflakes using the self-similar Rayleigh-Gans Approximation, Quarterly Journal of the Royal Meteorological Society, 143, 834–844, https://doi.org/10.1002/qj.2968, http://doi.wiley.com/10.1002/qj.2968, 2017.

Houze, R. A., McMurdie, L. A., Petersen, W. A., Schwaller, M. R., Baccus, W., Lundquist, J. D., Mass, C. F., Nijssen, B., Rutledge, S. A., Hudak, D. R., Tanelli, S., Mace, G. G., Poellot, M. R., Lettenmaier, D. P., Zagrodnik, J. P., Rowe, A. K., DeHart, J. C., Madaus, L. E., Barnes, H. C., and Chandrasekar, V.: The Olympic Mountains Experiment (OLYMPEX), Bulletin of the American Meteorological Society, 98, 2167–2188, https://doi.org/10.1175/BAMS-D-16-0182.1, http://journals.ametsoc.org/doi/10.1175/BAMS-D-16-0182.1, 2017.

Illingworth, A. J. and Blackman, T. M.: The Need to Represent Raindrop Size Spectra as Normalized Gamma Distributions for the Interpretation of Polarization Radar Observations, Journal of Applied Meteorology, 41, 286–297, https://doi.org/10.1175/1520-0450(2002)041<0286:TNTRRS>2.0.CO;2, http://journals.ametsoc.org/doi/abs/10.1175/1520-0450(2002)041<0286:TNTRRS>2.0.CO;2, 2002.

Illingworth, A. J., Barker, H. W., Beljaars, A., Ceccaldi, M., Chepfer, H., Clerbaux, N., Cole, J., Delanoë, J., Domenech, C., Donovan, D. P., Fukuda, S., Hirakata, M., Hogan, R. J., Huenerbein, A., Kollias, P., Kubota, T., Nakajima, T., Nakajima, T. Y., Nishizawa, T., Ohno, Y., Okamoto, H., Oki, R., Sato, K., Satoh, M., Shephard, M. W., Velázquez-Blázquez, A., Wandinger, U., Wehr, T., and van Zadelhoff, G.-J.: The EarthCARE Satellite: The Next Step Forward in Global Measurements of Clouds, Aerosols, Precipitation, and Radiation, Bulletin of the American Meteorological Society, 96, 1311–1332, https://doi.org/10.1175/BAMS-D-12-00227.1, http://journals.ametsoc.org/doi/abs/10.1175/BAMS-D-12-00227.1, 2015.

Kalesse, H., Szyrmer, W., Kneifel, S., Kollias, P., and Luke, E.: Fingerprints of a riming event on cloud radar Doppler spectra: observations and modeling, Atmospheric Chemistry and Physics, 16, 2997–3012, https://doi.org/10.5194/acp-16-2997-2016, http://www.atmos-chem-phys.net/16/2997/2016/, 2016.

Kneifel, S., Kulie, M. S., and Bennartz, R.: A triple-frequency approach to retrieve microphysical snowfall parameters, Journal of Geophysical Research Atmospheres, https://doi.org/10.1029/2010JD015430, 2011.

Kneifel, S., von Lerber, A., Tiira, J., Moisseev, D., Kollias, P., and Leinonen, J.: Observed relations between snowfall microphysics and triple-frequency radar measurements, Journal of Geophysical Research: Atmospheres, 120, 6034–6055, https://doi.org/10.1002/2015JD023156, http://doi.wiley.com/10.1002/2015JD023156http://onlinelibrary.wiley.com/doi/10.1002/2015JD023156/full, 2015.

Kneifel, S., Kollias, P., Battaglia, A., Leinonen, J., Maahn, M., Kalesse, H., and Tridon, F.: First observations of triple-frequency radar Doppler spectra in snowfall: Interpretation and applications, Geophysical Research Letters, 43, 2225–2233, https://doi.org/10.1002/2015GL067618, http://doi.wiley.com/10.1002/2015GL067618https://agupubs.onlinelibrary.wiley.com/doi/abs/10.1002/2015GL067618, 2016.

Kneifel, S., Dias Neto, J., Ori, D., Moisseev, D., Tyynelä, J., Adams, I. S., Kuo, K.-S., Bennartz, R., Berne, A., Clothiaux, E. E., Eriksson, P., Geer, A. J., Honeyager, R., Leinonen, J., and Westbrook, C. D.: Summer Snowfall Workshop: Scattering Properties of Realistic Frozen Hydrometeors from Simulations and Observations, as well as Defining a New Standard for Scattering Databases, Bulletin of the American Meteorological Society, 99, ES55–ES58, https://doi.org/10.1175/BAMS-D-17-0208.1, http://journals.ametsoc.org/doi/10.1175/BAMS-D-17-0208.1, 2018.

Langleben, M. P.: The terminal velocity of snowflakes, Quarterly Journal of the Royal Meteorological Society, 80, 174–181, https://doi.org/10.1002/qj.49708034404, http://doi.wiley.com/10.1002/qj.49708034404, 1954.

Leinonen, J. and Moisseev, D. N.: What do triple-frequency radar signatures reveal about aggregate snowflakes?, Journal of Geophysical Research: Atmospheres, 120, 229–239, https://doi.org/10.1002/2014JD022072, http://onlinelibrary.wiley.com/doi/10.1002/2014JD022072/fullhttp://doi.wiley.com/10.1002/2014JD022072, 2015.

Leinonen, J. and Szyrmer, W.: Radar signatures of snowflake riming: A modeling study, Earth and Space Science, 2, 346–358, https://doi.org/10.1002/2015EA000102, http://onlinelibrary.wiley.com/doi/10.1002/2015EA000102/fullhttp://doi.wiley.com/10.1002/2015EA000102, 2015.

Leinonen, J., Moisseev, D. N., Chandrasekar, V., and Koskinen, J.: Mapping Radar Reflectivity Values of Snowfall Between Frequency Bands, IEEE Transactions on Geoscience and Remote Sensing, 49, 3047–3058, https://doi.org/10.1109/TGRS.2011.2117432, https://ieeexplore.ieee.org/abstract/document/5738680/http://ieeexplore.ieee.org/document/5738680/, 2011.

Leinonen, J., Kneifel, S., Moisseev, D. N., Tyynelä, J., Tanelli, S., and Nousiainen, T.: Evidence of nonspheroidal behavior in millimeter-wavelength radar observations of snowfall, Journal of Geophysical Research: Atmospheres, 117, n/a–n/a, https://doi.org/10.1029/2012JD017680, http://doi.wiley.com/10.1029/2012JD017680, 2012.

Leinonen, J., Kneifel, S., and Hogan, R. J.: Evaluation of the Rayleigh-Gans approximation for microwave scattering by rimed snowflakes, Quarterly Journal of the Royal Meteorological Society, 144, 77–88, https://doi.org/10.1002/qj.3093, http://doi.wiley.com/10.1002/qj.3093, 2018a.

Leinonen, J., Lebsock, M. D., Tanelli, S., Sy, O. O., Dolan, B., Chase, R. J., Finlon, J. A., von Lerber, A., and Moisseev, D.: Retrieval of snowflake microphysical properties from multifrequency radar observations, Atmospheric Measurement Techniques, 11, 5471–5488, https://doi.org/10.5194/amt-11-5471-2018, https://www.atmos-meas-tech.net/11/5471/2018/, 2018b.

Li, H., Moisseev, D., and von Lerber, A.: How Does Riming Affect Dual-Polarization Radar Observations and Snowflake Shape?, Journal of Geophysical Research: Atmospheres, 123, 6070–6081, https://doi.org/10.1029/2017JD028186, http://doi.wiley.com/10.1029/2017JD028186, 2018.

Maahn, M. and Löhnert, U.: Potential of Higher-Order Moments and Slopes of the Radar Doppler Spectrum for Retrieving Microphysical and Kinematic Properties of Arctic Ice Clouds, Journal of Applied Meteorology and Climatology, 56, 263–282, https://doi.org/10.1175/JAMC-D-16-0020.1, http://journals.ametsoc.org/doi/10.1175/JAMC-D-16-0020.1, 2017.

Mace, G. and Benson, S.: Diagnosing Cloud Microphysical Process Information from Remote Sensing Measurements—A Feasibility Study Using Aircraft Data. Part I: Tropical Anvils Measured during TC4, Journal of Applied Meteorology and Climatology, 56, 633–649, https://doi.org/10.1175/JAMC-D-16-0083.1, http://journals.ametsoc.org/doi/10.1175/JAMC-D-16-0083.1, 2017.

Marshall, J. S. J. and Palmer, W. M. K.: The distribution of raindrops with size, Journal of Meteorology, 5, 165–166, https://doi.org/10.1175/1520-0469(1948)005<0165:TDORWS>2.0.CO;2, 1948.

Mason, S. L., Chiu, J. C., Hogan, R. J., and Tian, L.: Improved rain rate and drop size retrievals from airborne Doppler radar, Atmospheric Chemistry and Physics, 17, 11 567–11 589, https://doi.org/10.5194/acp-17-11567-2017, https://www.atmos-chem-phys.net/17/11567/2017/, 2017.

Mason, S. L., Chiu, C. J., Hogan, R. J., Moisseev, D., and Kneifel, S.: Retrievals of Riming and Snow Density From Vertically Pointing Doppler Radars, Journal of Geophysical Research: Atmospheres, 123, 807–13, https://doi.org/10.1029/2018JD028603, http://doi.wiley.com/10.1029/2018JD028603https://onlinelibrary.wiley.com/doi/abs/10.1029/2018JD028603, 2018.

Mitchell, D. L. and Heymsfield, A. J.: Refinements in the Treatment of Ice Particle Terminal Velocities, Highlighting Aggregates, Journal of the Atmospheric Sciences, 62, 1637–1644, https://doi.org/10.1175/JAS3413.1, http://journals.ametsoc.org/doi/abs/10.1175/JAS3413.1, 2005.

Moisseev, D., von Lerber, A., and Tiira, J.: Quantifying the effect of riming on snowfall using ground-based observations, Journal of Geophysical Research: Atmospheres, 122, https://doi.org/10.1002/2016JD026272, http://doi.wiley.com/10.1002/2016JD026272, 2017.

Moisseev, D. N. and Chandrasekar, V.: Examination of the μ–Λ Relation Suggested for Drop Size Distribution Parameters, Journal of Atmospheric and Oceanic Technology, 24, 847–855, https://doi.org/10.1175/JTECH2010.1, 2007.

Mosimann, L.: An improved method for determining the degree of snow crystal riming by vertical Doppler radar, Atmospheric Research, 37, 305–323, https://doi.org/10.1016/0169-8095(94)00050-N, http://www.sciencedirect.com/science/article/pii/016980959400050N, 1995.

National Academies of Sciences Engineering and Medicine: Thriving on Our Changing Planet: A Decadal Strategy for Earth Observation from Space, National Academies Press, Washington, D.C., https://doi.org/10.17226/24938, https://www.nap.edu/catalog/24938, 2018.

Newman, A. J., Kucera, P. A., and Bliven, L. F.: Presenting the Snowflake Video Imager (SVI), Journal of Atmospheric and Oceanic Technology, 26, 167–179, https://doi.org/10.1175/2008JTECHA1148.1, http://journals.ametsoc.org/doi/abs/10.1175/2008JTECHA1148.1, 2009.

Petäjä, T., O'Connor, E. J., Moisseev, D., Sinclair, V. A., Manninen, A. J., Väänänen, R., von Lerber, A., Thornton, J. A., Nicoll, K., Petersen, W., Chandrasekar, V., Smith, J. N., Winkler, P. M., Krüger, O., Hakola, H., Timonen, H., Brus, D., Laurila, T., Asmi, E., Riekkola, M.-L., Mona, L., Massoli, P., Engelmann, R., Komppula, M., Wang, J., Kuang, C., Bäck, J., Virtanen, A., Levula, J., Ritsche, M., and Hickmon, N.: BAECC: A Field Campaign to Elucidate the Impact of Biogenic Aerosols on Clouds and Climate, Bulletin of the American Meteorological Society, 97, 1909–1928, https://doi.org/10.1175/BAMS-D-14-00199.1, http://journals.ametsoc.org/doi/10.1175/BAMS-D-14-00199.1, 2016.

Sinclair, V. A., Moisseev, D., and von Lerber, A.: How dual-polarization radar observations can be used to verify model representation of secondary ice, Journal of Geophysical Research: Atmospheres, 121, 954–10, https://doi.org/10.1002/2016JD025381, http://doi.wiley.com/10.1002/2016JD025381, 2016.

Stein, T. H. M., Westbrook, C. D., and Nicol, J. C.: Fractal geometry of aggregate snowflakes revealed by triple-wavelength radar measurements, Geophysical Research Letters, 42, 176–183, https://doi.org/10.1002/2014GL062170, http://doi.wiley.com/10.1002/2014GL062170, 2015.

Szyrmer, W. and Zawadzki, I.: Snow Studies. Part III: Theoretical Derivations for the Ensemble Retrieval of Snow Microphysics from Dual-Wavelength Vertically Pointing Radars, Journal of the Atmospheric Sciences, 71, 1158–1170, https://doi.org/10.1175/JAS-D-12-0285.1, http://journals.ametsoc.org/doi/abs/10.1175/JAS-D-12-0285.1, 2014a.

Szyrmer, W. and Zawadzki, I.: Snow Studies. Part IV: Ensemble Retrieval of Snow Microphysics from Dual-Wavelength Vertically Pointing Radars, Journal of the Atmospheric Sciences, 71, 1171–1186, https://doi.org/10.1175/JAS-D-12-0286.1, http://journals.ametsoc.org/doi/abs/10.1175/JAS-D-12-0286.1, 2014b.

Testud, J., Oury, S., Black, R. A., Amayenc, P., and Dou, X.: The Concept of "Normalized" Distribution to Describe Raindrop Spectra: A Tool for Cloud Physics and Cloud Remote Sensing, Journal of Applied Meteorology, 40, 1118–1140, https://doi.org/10.1175/1520-0450(2001)040<1118:TCONDT>2.0.CO;2, http://journals.ametsoc.org/doi/abs/10.1175/1520-0450(2001)040<1118:TCONDT>2.0.CO;2, 2001.

Tiira, J., Moisseev, D. N., von Lerber, A., Ori, D., Tokay, A., Bliven, L. F., and Petersen, W.: Ensemble mean density and its connection to other microphysical properties of falling snow as observed in Southern Finland, Atmospheric Measurement Techniques, 9, 4825–4841, https://doi.org/10.5194/amt-9-4825-2016, http://www.atmos-meas-tech.net/9/4825/2016/, 2016.

Tridon, F., Battaglia, A., Chase, R. J., Truk, F. J., Leinonen, J., Kneifel, S., Mroz, K., Finlon, J., Bansemer, A., Tanelli, S., Heymsfield, A. J., and Nesbitt, S. W.: The microphysics of stratiform precipitation during OLYMPEx:compatibility between 3-frequency radar and airborne in situ observations, Journal of Geophysical Research: Atmospheres, 2019.

von Lerber, A., Moisseev, D., Bliven, L. F., Petersen, W., Harri, A.-M., and Chandrasekar, V.: Microphysical Properties of Snow and Their Link to Ze-S Relations during BAECC 2014, Journal of Applied Meteorology and Climatology, 56, 1561–1582, https://doi.org/10.1175/JAMC-D-16-0379.1, http://journals.ametsoc.org/doi/10.1175/JAMC-D-16-0379.1, 2017.

Westbrook, C. D., Ball, R. C., Field, P. R., and Heymsfield, A. J.: Universality in snowflake aggregation, Geophysical Research Letters, 31, L15 104, https://doi.org/10.1029/2004GL020363, http://doi.wiley.com/10.1029/2004GL020363, 2004.

Williams, C. R., Bringi, V. N., Carey, L. D., Chandrasekar, V., Gatlin, P. N., Haddad, Z. S., Meneghini, R., Joseph Munchak, S., Nesbitt, S. W., Petersen, W. A., Tanelli, S., Tokay, A., Wilson, A., Wolff, D. B., Williams, C. R., Bringi, V. N., Carey, L. D., Chandrasekar, V., Gatlin, P. N., Haddad, Z. S., Meneghini, R., Munchak, S. J., Nesbitt, S. W., Petersen, W. A., Tanelli, S., Tokay, A., Wilson, A., and Wolff, D. B.: Describing the Shape of Raindrop Size Distributions Using Uncorrelated Raindrop Mass Spectrum Parameters, Journal of Applied Meteorology and Climatology, 53, 1282–1296, https://doi.org/10.1175/JAMC-D-13-076.1, http://journals.ametsoc.org/doi/abs/10.1175/JAMC-D-13-076.1, 2014.

Data availability. AMF2 remote-sensed data from BAECC 2014 are available from the ARM data archive (https://www.arm.gov/data). PIP video disdrometer measurements from Hyytiälä can be accessed at github (https://github.com/dmoisseev/Snow-Retrievals-2014-2015).

Appendix A: Retrieved profiles

The profiles of retrieved variables corresponding to the retrievals described in Section 4.2 are Fig. A1 for the ~~prefrontal~~ unrimed regime and Fig. A2 for the ~~frontal~~ rimed regime.

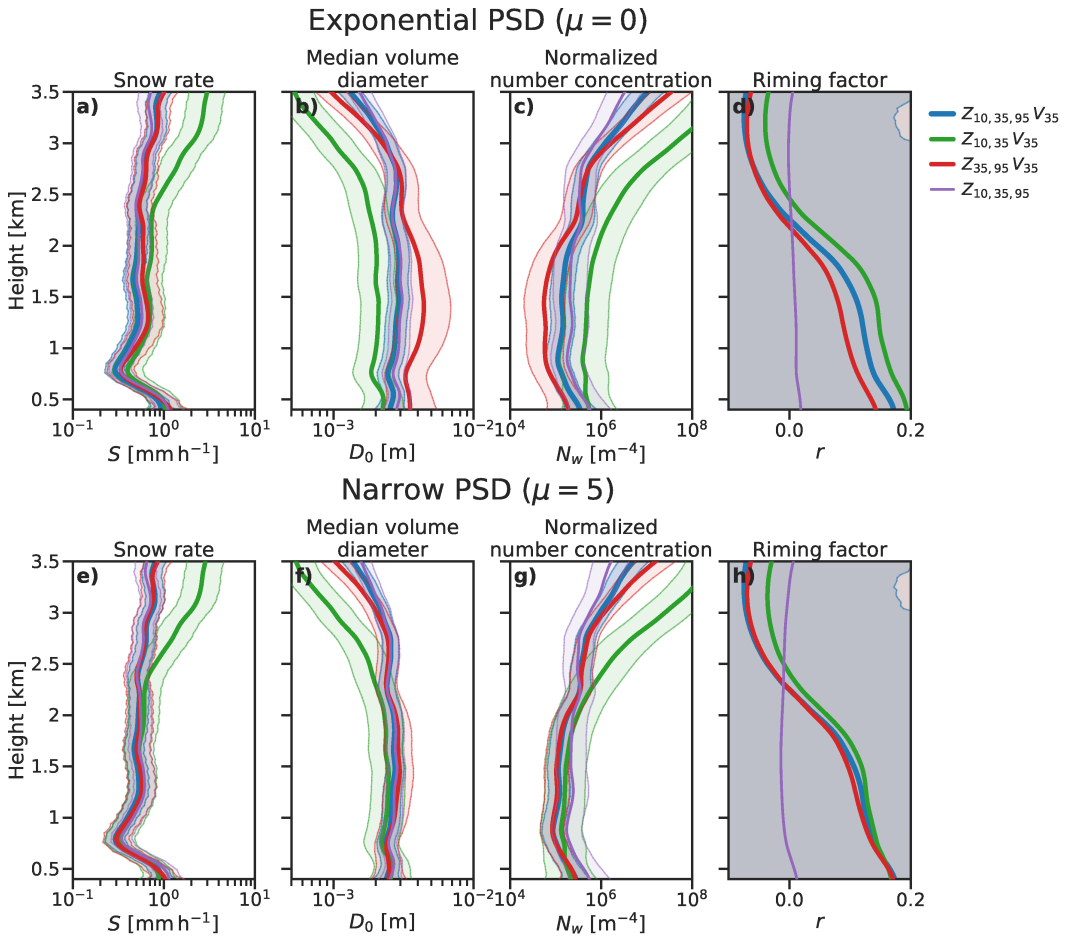

Figure A1. Profiles of retrieved variables for retrievals of a selected profile during the ~~prefrontal~~ rimed snow regime. Retrievals assuming (a–d) an exponential PSD are compared against those with (e–h) a narrow PSD with $\mu = 5$.

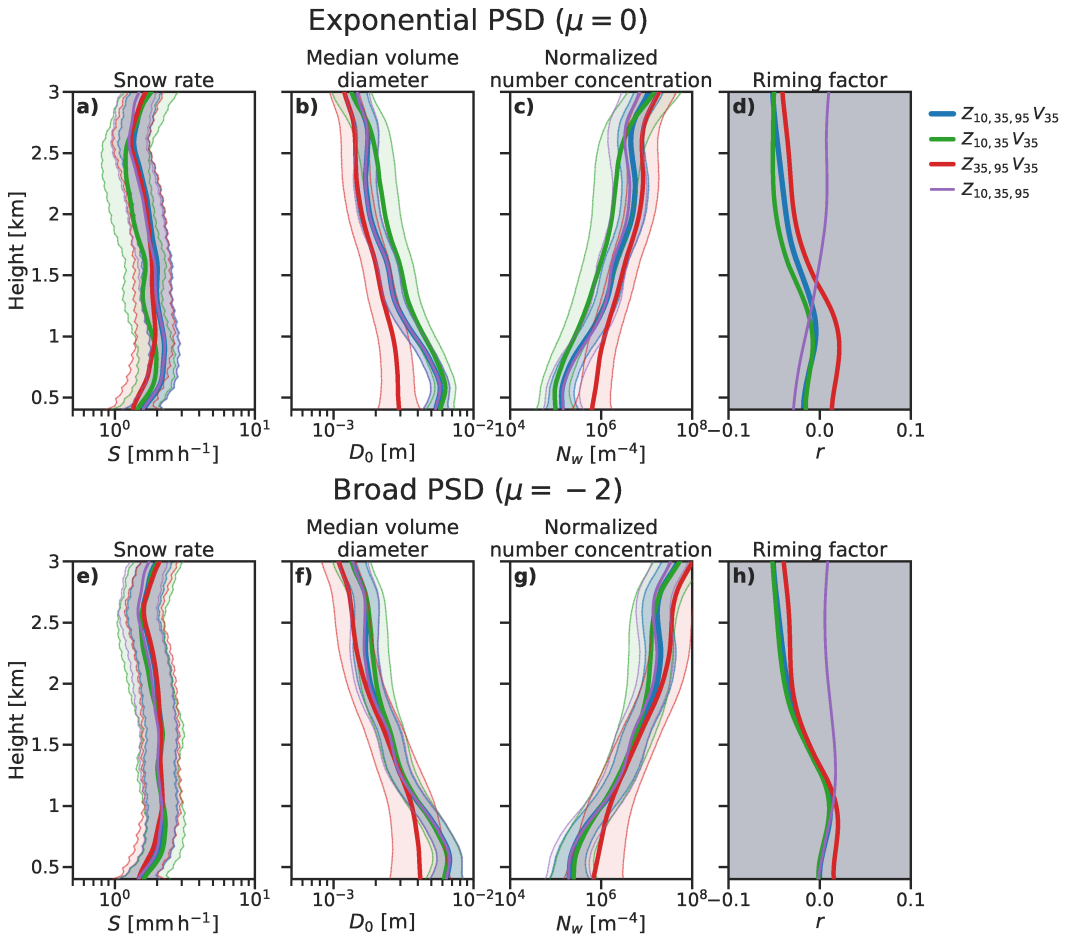

Figure A2. Profiles of retrieved variables for retrievals of a selected profile during the ~~frontal~~ unrimed snow regime. Retrievals assuming (a–b) an exponential PSD are compared against those with (e–h) a broad PSD with $\mu = -2$.

Author contributions.

Competing interests. The authors do not have any competing interests.

Acknowledgements. This work is supported by the National Centre for Earth Observation (NCEO) and European Space Agency Grant 4000112030/15/NL/CT, with computing resources provided by the University of Reading. D. Moisseev acknowledges funding from ERA-PLANET, transnational project iCUPE (Grant Agreement 689443), funded under the EU Horizon 2020 Framework Programme and Academy of Finland (grants 307331 and 305175). Contributions by S. Kneifel were carried out within the Emmy-Noether Group OPTIMIce funded by the German Science Foundation (DFG) under Grant KN 1112/2-1.